

PLOS Computational Biology
Do vascular networks branch optimally or randomly across spatial scales?
 --Manuscript Draft--

Manuscript Number:	
Full Title:	Do vascular networks branch optimally or randomly across spatial scales?
Short Title:	Are vascular networks optimized or random?
Article Type:	Research Article
Keywords:	Keywords: vascular branching; allometric scaling; optimal networks; random networks; branching angles
Corresponding Author:	Van M Savage University of California, Los Angeles Los Angeles, CA UNITED STATES
Corresponding Author Secondary Information:	
Corresponding Author's Institution:	University of California, Los Angeles
Corresponding Author's Secondary Institution:	
First Author:	Elif Tekin
First Author Secondary Information:	
Order of Authors:	Elif Tekin Mitchell G Newberry Van Savage
Order of Authors Secondary Information:	
Abstract:	Modern models that derive allometric relationships between metabolic rate and body mass are based on the architectural design of the cardiovascular system and presume sibling vessels are symmetric in terms of radius, length, flow rate, and pressure. Those models predict power-law or concave curvature as opposed to the convex curvature observed in empirical data. Here, we study the cardiovascular structure of human head and torso as well as mouse lung based on three-dimensional images processed via our software Angicart. We find systematic patterns of asymmetry in vascular branching that may help explain previously documented mismatches between predictions from scaling theory and data. To examine these mismatches, we construct a mathematical framework to derive predictions based on local, junction-level optimality principles that have been proposed to be favored in the course of natural selection and development. The two most commonly-used principles are material-cost optimizations (construction materials or blood volume) and optimization of efficient flow via minimization of power loss. We show that material-cost optimization solutions match with distributions for asymmetric branching across the whole network but do not match well for individual junctions. Consequently, we also explore random branching that is constrained at scales that range from local (node-level) to global (whole network). We find that material-cost optimizations are the strongest predictor of vascular branching in the human head and torso, whereas locally or intermediately constrained random branching is comparable to material-cost optimizations for the mouse lung. These differences could be attributable to developmentally-programmed local branching for larger vessels and constrained random branching for smaller vessels.
Suggested Reviewers:	Charles Price University of Western Australia charles.price@uwa.edu.au Chen Hou Missouri University of Science and Technology houch@mst.edu

	Melanie Moses University of New Mexico melaniem@unm.edu
	Eleni Katifori University of Pennsylvania katifori@sas.upenn.edu
	Carl Modes Rockefeller University cmodes@rockefeller.edu
	Mette Olufsen North Caroline State University msolufse@unity.ncsu.edu
Opposed Reviewers:	
Additional Information:	
Question	Response
Data Availability	Yes - all data are fully available without restriction
PLOS journals require authors to make all data underlying the findings described in their manuscript fully available, without restriction and from the time of publication, with only rare exceptions to address legal and ethical concerns (see the PLOS Data Policy and FAQ for further details). When submitting a manuscript, authors must provide a Data Availability Statement that describes where the data underlying their manuscript can be found. Your answers to the following constitute your statement about data availability and will be included with the article in the event of publication. Please note that simply stating 'data available on request from the author' is not acceptable. If, however, your data are only available upon request from the author(s), you must answer "No" to the first question below, and explain your exceptional situation in the text box provided.	
Do the authors confirm that all data underlying the findings described in their manuscript are fully available without restriction?	
Please describe where your data may be found, writing in full sentences. Your answers should be entered into the box below and will be published in the form you provide them, if your manuscript is accepted. If you are copying our sample text below, please ensure you replace any instances of XXX with the appropriate details.	Human head and torso vascular data are included in the software distribution at https://github.com/mnewberry/angicart . Mouse lung vascular data will be included in the https://github.com/mnewberry/angicart upon acceptance of the manuscript.

If your data are all contained within the paper and/or Supporting Information files, please state this in your answer below. For example, "All relevant data are within the paper and its Supporting Information files."

If your data are held or will be held in a public repository, include URLs, accession numbers or DOIs. For example, "All XXX files are available from the XXX database (accession number(s) XXX, XXX)." If this information will only be available after acceptance, please indicate this by ticking the box below.

If neither of these applies but you are able to provide details of access elsewhere, with or without limitations, please do so in the box below. For example:

"Data are available from the XXX Institutional Data Access / Ethics Committee for researchers who meet the criteria for access to confidential data."

"Data are from the XXX study whose authors may be contacted at XXX."

* typeset

Additional data availability information:

Tick here if the URLs/accession numbers/DOIs will be available only after acceptance of the manuscript for publication so that we can ensure their inclusion before publication.

UNIVERSITY OF CALIFORNIA, LOS ANGELES

BERKELEY • DAVIS • IRVINE • LOS ANGELES • MERCED • RIVERSIDE • SAN DIEGO • SAN FRANCISCO

UCLA



SANTA BARBARA • SANTA CRUZ

DEPARTMENT OF BIOMATHEMATICS
 DAVID GEFFEN SCHOOL OF MEDICINE AT UCLA
 621 CHARLES E. YOUNG DRIVE SOUTH
 ROOM 5303, LIFE SCIENCES
 BOX 951766
 LOS ANGELES, CALIFORNIA 90095-1766

FAX: (310) 825-8685

PLOS Computational Biology
 CARLYLE HOUSE
 CARLYLE ROAD
 CAMBRIDGE,CB4 3DN
 UNITED KINGDOM
 PHONE: +44 (0)1223 442 810 | FAX: +44 (0)1223 442 833

April 28, 2016

Dear Editors,

We are submitting a manuscript titled, “Do vascular networks branch optimally or randomly across spatial scales?” for consideration in PLOS *Computational Biology*. We use our software, Angicart (1, 2), to extract vascular data for human head and torso as well as mouse lung in order to characterize systematic patterns of asymmetric branching for the branching angles, radii, and lengths in animal vascular systems. Moreover, for the first time, we try to predict these patterns based on optimized versus randomized networks with constraints that range from local (single node or branching junction) to global (whole network) scales. Our analysis shows that the lengths of sibling vessels—vessels that come from the same branching junction and share the same parent—are highly asymmetric (i.e., have different values), while vessel radii and branching angles are skewed towards symmetry (i.e., vessels tend to have the same radii and branching angles). By comparing these empirical findings with several optimization models and simulations of random branching, we further show that local information is not enough to lead to the patterns of asymmetric branching that we observe, and that information is needed at larger spatial scales that incorporates downstream branching junctions and vessels.

Consequently, our paper represents two paradigm shifts in the understanding and modeling of vascular networks. First, it shows that length asymmetry is not a correction to an assumption of asymmetry but instead a pervasive, wide ranging, and uniform feature that requires a complete re-working of models. This finding is clearly established through our analysis of new and extensive empirical data from mouse lung and human head and torso. Second, it shows that the spatial scale at which models determine vascular branching needs to be extended and generalized from the level of a single branching junction to an intermediate level that incorporates a larger neighborhood of downstream vessels and branching junctions. This finding arises from several lines of evidence that include: 1. The fact that minimization of power loss predicts no branching at all for a single junction when there is asymmetric branching, 2. The finding that material-cost optimizations show good agreement with empirical data for asymmetry at the network level but not at the node (single branching junction) level, and 3. Simulations of random vascular branching that are constrained at intermediate spatial scales provide a reasonable match to empirical data.

Therefore, our results have the potential to dramatically impact current models and theories for vascular branching. In particular, most models assume symmetric branching—sibling vessels are identical in size and flow—that is optimized locally at each individual branching junction. Indeed, these assumptions have been used to famously derive the allometric scaling relationship between metabolic rate and body mass across species (3-7). We demonstrate that this assumption of symmetric branching is strongly violated and not even approximately true with regard to vessel lengths in mammalian vascular systems, echoing results for plant xylem vascular networks (8-10). This finding means that the mechanisms and mathematical forms of the space-filling principle in current models, which determine the scaling of vessel lengths, need to be changed. That is, they need to be re-envisioned to incorporate and predict these pervasive asymmetries in vessel lengths that characterize real systems while still allowing for symmetry in vessel radii and branching angles. Accomplishing this would help resolve current mismatches between scaling theory and curvature in empirical data for metabolic rate, and thus provide a more biologically-grounded and informed theory of vascular networks and allometric scaling.

To explore what factors cause these general patterns of asymmetry, we consider biological and physical constraints: 1) material-cost optimizations that effectively minimize the total construction material or minimize the total blood volume at the local bifurcation, and 2) power-cost optimizations that provide efficient distribution and flow of blood via minimization of total power loss at the local branching junction. Based on these optimality principles, we build mathematical models and derive predictions for asymmetric branching. Comparison of the theoretical predictions with empirical data shows that asymmetry patterns match material-cost optimizations at the level of the whole network reasonably well but match poorly at the individual junction level, suggesting the correct scale of optimization is not the local branching junction. These observations for the local optimizations direct us to explore different spatial scales for the formation of the vascular branching. In so doing, we produce random networks across four different spatial scales that range from local to global. That is, branching junctions are randomly placed according to different degrees of spatial constraints. This analysis leads us to conclude that intermediate spatial scales are likely the correct level of spatial constraints. Fascinatingly, we find that material-cost optimizations provide the best prediction for the human head and torso branching, whereas locally or intermediately constrained random branching offers the greatest match with the mouse lung data across all models. We argue this is because the larger vessels in the human head and torso may be more evolutionarily constrained and developmentally programmed, while small vessels in the mouse lung may be free to branch more randomly so long as the space is filled.

Our article should be of interest to computational biologists, mathematical biologists, vascular biologists, physiologists, and the wide range of scientists interested in allometric scaling (e.g., macroecologists, oncologists interested in angiogenesis and tumor growth, and many more). In our paper, we use novel software, statistically analyze large datasets, develop mathematical models and derive predictions, perform stochastic simulations, and compare results from all these methods to arrive at new and compelling biological insights.

To review this article, we recommend

Charles Price (charles.price@uwa.edu.au)
Chen Hou (houch@mst.edu)
Melanie Moses (melaniem@unm.edu)
Eleni Katifori (katifori@sas.upenn.edu)
Carl Modes (cmodes@rockefeller.edu)

Mette Olufsen (msolufse@unity.ncsu.edu)

Thank you for your consideration.

Sincerely,

Elif Tekin and Van Savage

References

1. Newberry M. Code for angicart software 2011 [Available from: github.com/mnewberry/angicart].
2. Newberry MG, Ennis DB, Savage VM. Testing Foundations of Biological Scaling Theory Using Automated Measurements of Vascular Networks. *PLoS Comput Biol*. 2015;11(8):e1004455.
3. West GB, Brown JH, Enquist BJ. A General Model for the Origin of Allometric Scaling Laws in Biology. *Science*. 1997;276:122-6.
4. Banavar JR, Cooke TJ, Rinaldo A, Maritan A. Form, function, and evolution of living organisms. *Proceedings of the National Academy of Sciences*. 2014;111(9):3332-7.
5. Banavar JR, Maritan A, Rinaldo A. Size and Form in Efficient Transportation Networks. *Nature*. 1999;399:130-2.
6. Dodds PS. Optimal form of branching supply and collection networks. *Physical review letters*. 2010;104(4):048702.
7. Huo Y, Kassab GS. Intraspecific scaling laws of vascular trees. *Journal of The Royal Society Interface*. 2012;9(66):190-200.
8. Price CA, Symonova O, Mileyko Y, Hilley T, Weitz JS. Leaf extraction and analysis framework graphical user interface: Segmenting and analyzing the structure of leaf veins and areoles. *Plant Physiology*. 2011;155(1):236.
9. Mileyko Y, Edelsbrunner H, Price CA, Weitz JS. Hierarchical ordering of reticular networks. *PLoS One*. 2012;in press.
10. Scoffoni C, Rawls M, McKown A, Cochard H, Sack L. Decline of leaf hydraulic conductance with leaf hydration: relationship to leaf size and venation architecture. *Plant Physiology*. 2011;156:832-43.

1 Do vascular networks branch optimally or randomly across spatial scales?

2

3 Elif Tekin¹, Mitchell G. Newberry², Van M. Savage^{*1, 3, 4}

4

5

6 ¹Department of Biomathematics, University of California, David Geffen School of
7 Medicine, Los Angeles, CA 90095

8 ² Department of Biology, University of Pennsylvania, Philadelphia, PA 19104

9 ³Department of Ecology and Evolutionary Biology, University of California, Los Angeles,
10 CA 90095

11 ⁴Santa Fe Institute, Santa Fe, NM 87501

12

13 *Corresponding Author

14 E-mail: vsavage@ucla.edu

15

16

17 **Abstract**

18 Modern models that derive allometric relationships between metabolic rate and body
19 mass are based on the architectural design of the cardiovascular system and presume
20 sibling vessels are symmetric in terms of radius, length, flow rate, and pressure. Those
21 models predict power-law or concave curvature as opposed to the convex curvature
22 observed in empirical data. Here, we study the cardiovascular structure of human head
23 and torso as well as mouse lung based on three-dimensional images processed via our
24 software Angicart. We find systematic patterns of asymmetry in vascular branching that
25 may help explain previously documented mismatches between predictions from scaling
26 theory and data. To examine these mismatches, we construct a mathematical
27 framework to derive predictions based on local, junction-level optimality principles that
28 have been proposed to be favored in the course of natural selection and development.
29 The two most commonly-used principles are material-cost optimizations (construction
30 materials or blood volume) and optimization of efficient flow via minimization of power
31 loss. We show that material-cost optimization solutions match with distributions for
32 asymmetric branching across the whole network but do not match well for individual
33 junctions. Consequently, we also explore random branching that is constrained at
34 scales that range from local (node-level) to global (whole network). We find that
35 material-cost optimizations are the strongest predictor of vascular branching in the
36 human head and torso, whereas locally or intermediately constrained random branching
37 is comparable to material-cost optimizations for the mouse lung. These differences
38 could be attributable to developmentally-programmed local branching for larger vessels
39 and constrained random branching for smaller vessels.

40 **Keywords:** vascular branching; allometric scaling; optimal networks; random networks;
41 branching angles

42 **Author summary**

43 The architecture of vascular networks must balance complex demands to efficiently
44 deliver oxygen and resources throughout the entire body. These complex demands
45 constrain the possible forms of vasculature. Because of these constraints and the
46 indispensable role of vasculature for much of life, scientists have sought to identify
47 systematic patterns in the structural properties of vascular networks and whether these
48 can be predicted from models based on biological and physical principles. These
49 studies have been limited by the lack of extensive, detailed data. Using high-quality
50 vascular network data obtained via our software, Angicart, we identify novel, systematic
51 patterns of asymmetry in sizes and branching angles among sibling vessels from mouse
52 lung and human head and torso. To examine what constraints might underlie these
53 patterns, we investigate several explanations, including various types of optimal
54 branching as well as random branching. The optimal branchings were derived locally
55 with respect to constraints on material costs or power loss. For random branching we
56 allowed the degree of randomness to vary from local to global spatial scales. By
57 comparing predictions with real data, our study suggests that key components in
58 determining vascular branching are material costs along with some randomness at local
59 to intermediate spatial scales.

60 **1. Introduction**

61 The cardiovascular system is responsible for the vital processes of delivering oxygen
62 and nutrients to cells, as well as clearing waste products, via blood flow from heart to
63 capillaries. Accomplishing these processes requires highly complex structures because
64 nearly all the cells throughout the body are fed by capillaries—the terminal tips of the
65 cardiovascular system.

66 These linkages explain why the cardiovascular system plays a critical role in
67 most modern allometric scaling theories that relate metabolic rate and body mass via a
68 power law with the scaling exponent 3/4 (1-8). Recent analyses of allometric scaling
69 relationships using extensive data (more than 600 mammalian species and 64 plant
70 species) yield second-order curvature in log-log space that represent deviations from
71 this pure power law (9-13). Attempts to account for this observed curvature, via
72 including higher-order approximations and more accurate fluid dynamic relations, lead
73 to curvature in the opposite direction (convex versus concave) of the empirical data (4).
74 These and other recent results suggest the need for a revised theory.

75 Current theories, such as those proposed by West, Brown, and Enquist (WBE)
76 (5), Banavar et al. (14, 15), Dodds (16), and Huo and Kassab (17) for allometric scaling
77 rely on mathematical models that encompass the architectural design of the
78 cardiovascular system to different degrees of detail and accuracy. Within these models,
79 the cardiovascular system is typically idealized as a hierarchical branching network that
80 is constrained by a few core physical and biological principles. These principles lead to
81 derivations for fractal-like, self-similar properties—a pattern that repeats itself across

82 large and small scales—for the overall structure of the network (18-20). Previous
83 models also often assume that branching is symmetric such that sibling vessels—
84 daughter vessels branching from the same parent—are identical in terms of their radius,
85 length, flow rate, and pressure.

86 Although many models presume perfect symmetry between siblings (5, 9, 17,
87 21), inspection of vessel casts and images reveals that some regions have highly
88 asymmetric branching (22-25). Such asymmetric branching patterns were empirically
89 quantified by Zamir who showed there are differing degrees of asymmetry across levels
90 of the coronary arteries (20, 26). Moreover, a recent paper by Hunt et al. (27) shows
91 that there is a high degree of asymmetry in vessel lengths within the mouse lungs
92 (micro-CT images) and human head and torso (MRI), convincingly demonstrating that
93 symmetric branching is not an accurate representation of the cardiovascular system.
94 Nevertheless, if the degree of asymmetry is repeated across branching junctions, this
95 would still represent a modified version of self-similarity.

96 Given the evidence for asymmetric branching, we propose to investigate patterns
97 of asymmetry in vascular branching. Because vessel radii exhibit relatively little
98 asymmetry and are consistent with existing models (28), we focus on asymmetries in
99 vessel lengths and branching angles. Through the identification and investigation of
100 these new, systematic patterns, an explanation might eventually be obtained for the
101 mismatch between theoretical predictions from scaling theory and empirical data.
102 Conversely, the consistency of the empirical scaling relationships across different
103 species and taxa (4, 8, 9, 11, 12) suggests that shared evolutionary pressures and
104 developmental processes powerfully constrain the degree of asymmetric branching

105 within the vascular system, possibly corresponding to core, yet unidentified, biological
106 and physical principles. For instance, it has been proposed that the architecture of the
107 cardiovascular system is governed by optimization principles such as minimization of
108 the construction materials (i.e. material cost (MC)) or of power loss (i.e. power cost
109 (PC)) across the network to provide efficient flow (29-33).

110 These evolutionary principles could constrain the branching structure locally
111 (individual branching junction), globally (whole network), or through some intermediate
112 spatial scale. The local optimization of these properties at each branching junction—
113 where a parent vessel branches into daughter vessels—has been studied by Murray
114 and Zamir for the case that the radii of vessels are fixed (29, 30, 33, 34). These
115 optimization problems were used to derive predictions for branching angles of sibling
116 vessels relative to the parent vessel (Fig 1c). Although not explicitly considered in
117 previous studies, length asymmetry is directly tied to branching angles because both
118 are completely determined by the position of the branching junction relative to the other
119 endpoints of the vessels. Furthermore, these previous studies incorrectly used a linear
120 summation of each vessel's individual power loss to calculate total power loss for the
121 branching junction (29, 30). This approach works for construction material but does not
122 for power loss because it ignores different rules for how to combine
123 resistances/impedances of vessels in parallel versus in series. Moreover, even for
124 minimization of material cost, these studies (29, 30, 33) did not examine the full solution
125 space for the optimal position of the branching junction, resulting in misleading solutions
126 for some cases. In this paper, we address these problems and clarify the confusion in
127 the literature on optimal branching geometries. In so doing, we provide a connection

128 between optimal branching angles, optimal ratios and asymmetries for sibling vessel
129 lengths, and observed asymmetry in branching patterns.

130 Although there are substantial theoretical predictions for the vascular system,
131 those predictions have rarely been tested on an extensive set of data. Most vascular
132 data have been collected via casting or dyeing methods (35-38) that do not produce
133 sufficiently detailed or large enough amounts of data due to the challenges of manually
134 measuring branching angles. Recently, a novel software package, Angicart, was
135 developed to extract three-dimensional vascular networks from the aligned stacks of
136 high quality angiographic images (28, 39). In this paper, we employ Angicart to analyze
137 characteristics of the cardiovascular structure from micro-CT images of healthy mouse
138 lung (Fig 1a) (micro-CT imaging is described in (40)) as well as the MRI of human head
139 and torso in 18 different subjects (Fig 1b) (27, 28). Consequently, we have collected
140 detailed data for vascular networks that includes measures of branching angles at each
141 junction.

142 Here, we first present patterns that hold across the entire network for the degree
143 of asymmetry in vessel radius, length, and branching angle between sibling vessels.

144 Then, we investigate the validity of the previously proposed branching angle
145 optimizations at the local level. As part of this, we propose an alternate method for
146 solving these minimization problems, including the full solution of the MC optimization
147 that considers both total surface area and total volume. Next, we introduce an
148 optimization scheme for minimizing power loss (i.e., PC optimization) that correctly
149 implements the flow dynamics for a bifurcating structure and can also incorporate
150 downstream impedances and power loss. We note that several of these optimization

151 schemes result in network-level patterns of asymmetry similar to those observed in the
152 real data. Next, as a stronger test of which optimization principles, if any, lead to the
153 asymmetric branching patterns in real systems, we compute theoretical predictions for
154 each branching junction in a comprehensive set of vascular data from mouse and
155 human subjects and compare whether our predictions match the real data at the
156 junction-level. Finally, we explore how random branching constrained at different spatial
157 scales, ranging from local to intermediate to global, affects the network-level
158 characteristics of the empirical data via simulations of the branching structure. Our
159 carefully constructed mathematical framework accompanied with a comparison to
160 empirical data enables us to improve our understanding of how structural properties of
161 the vascular system are constrained by core biological and physical principles.

162 **2. Optimal Models and Random Simulations for Vascular Branching**

163 **2.1. General framework for branching angle optimization and asymmetry**

164 Systematic patterns in branching angles or asymmetric ratios (27, 41-43) (see Results,
165 section 3.1) suggest a constraint that likely arises through natural selection, the nature
166 of the growth process, or both. Most hypotheses about the force of natural selection on
167 vasculature have focused on principles that reduce the cost of materials and growth
168 while also providing efficient flow mechanisms (26, 30-33). These biological principles
169 could apply at each branching junction (locally) during growth or across the whole
170 network (globally) through some larger bauplan. In this study, we initially focus on the
171 local optimization aspects of these principles. Then, we consider applying different
172 regional constraints on the branching structure, including simulating networks that have

173 random branching within constraints that range from intermediate to global spatial levels
174 of the network.

175 For the local optimization, following a similar approach as in the previous studies
176 by Zamir and Murray (29, 30, 33), we assume that the radius (r_i) and the unshared
177 endpoints of the vessels (V_i) are fixed, whereas the branching junction at the shared
178 endpoint (J) varies (Fig 1c, Fig A1). In this framework, we derive the optimal placement
179 of the branching junction by constructing and minimizing a cost function based on each
180 biological principle that is hypothesized to increase the fitness.

181 To try to elucidate the high degree of length asymmetry observed in data (see
182 Results 3.1), we also take a new approach and derive the length asymmetry from the
183 solutions of these optimization principles. That is, by finding optimal branching angle
184 solutions, we determine the location of the branching junction that in turn uniquely
185 determines vessel lengths and leads to predictions for optimal length asymmetry. The
186 formula that associates the length asymmetry with the optimal branching angles is
187 introduced in the Appendix A.

188 As mentioned above, we consider two general principles. First, because
189 construction and maintenance can be expensive to the body, minimizing total material is
190 a potential driving factor for the structure of the vascular system. Such principles will be
191 referred to as *material-cost optimizations* (MC). The total material cost across the
192 bifurcation is the linear sum of the material cost for each vessel because material cost is
193 an additive quantity over different vessels.

194 Next, a viable design for the vascular system requires efficient flow
195 mechanisms—such as minimal power loss—to transport nutrients and oxygen to cells.
196 This scheme will be called *power-cost optimization* (PC). In order to establish a cost
197 function that represents the total power loss across a bifurcation, we need to use
198 appropriate fluid-dynamical concepts. Because the effective impedance is not a linearly
199 additive quantity for combining vessels at a branching junction, PC optimization requires
200 a more complicated cost function than MC optimization. In this respect, our derivation
201 differs from and corrects previous branching angle optimizations by Zamir (29, 30). As
202 another new element to our approach, we further propose an optimization scheme that
203 can incorporate the power cost due to the downstream impedances beyond just a single
204 branching junction.

205 In all our derivations, we follow Krogh's model that regards blood vessels as
206 cylinders (44, 45). In addition, both human and mouse data provide evidence that all of
207 the vessels at a branching junction lie within a single plane (Fig S1). Thus, for our
208 derivations we assume that the branching junction lies in the plane determined by the
209 unshared endpoints of the vessels.

210 In the following sections, we first introduce the branching angle optimization
211 solutions for the MC and PC optimizations for a local branching junction. Next, we
212 explain a new scheme for the power-cost optimization that incorporates information
213 about the flow properties of the downstream vessels. Lastly, we relax the optimization
214 principles and present simulations of random branching to explore how local to
215 intermediate and global constraints can alone affect the characteristics of the vascular
216 network.

217 **2.2. Material-cost optimizations (MC)**

218 There are two types of material that are needed for the vascular system, blood vessels
219 (endothelial cells) and blood (plasma and white and red blood cells). The amount of
220 material necessary for vessel construction primarily depends on the surface-area of the
221 vessel: $2\pi r l$. In contrast, the material devoted to the blood is proportional to the blood
222 volume ($\pi r^2 l$). MC optimizations can be built upon these two different characteristics
223 (surface-area (MC-SA) or volume (MC-V)). We consider both cases here.

224 To consider total surface-area and volume as distinct structural constraints that
225 need to be minimized to conserve construction material, as in Murray and Zamir (29, 30,
226 33), we form a generic cost function H in which lengths are weighted according to the
227 corresponding optimization. Explicitly, $H = \sum_i h_i l_i$ where $h_i = 2\pi r_i$ for surface-area and
228 $h_i = \pi r_i^2$ for volume. In general, the constant geometric factors like 2π can be ignored
229 because they cancel from every term when the derivative of H is set equal to zero. For
230 fixed radii the material-cost optimization problem is equivalent to the weighted Fermat
231 Problem introduced by Greenberg and Robertello (46-48).

232 To solve these minimization problems, we present a different method than that
233 used to obtain Zamir and Murray's solutions. Our method relies on distance metrics
234 without invoking a coordinate system (Appendix B) and is therefore more simple and
235 general. The method is straightforward when it is realized that the location of the
236 branching junction is uniquely defined by the parent vessel length (l_0) and the angle
237 (φ_1) at the intersection of the parent vessel and one of its daughter vessels (Fig 1c, Fig

238 A1). Based on this, we obtain the full solution of optimal branching angles by finding the
239 stationary and singular points of H with respect to l_0 and φ_1 throughout the entire space.

240 In this framework, we recognize that the first order derivatives of H are
241 discontinuous and thus undefined at the unshared end points (V_0, V_1, V_2). Hence,
242 singularities (values of infinity) are attained at these end points. Moreover, we find that
243 the stationary solution for minimizing H exists only in the interior of the triangle defined
244 by the unshared endpoints. In the latter case, the optimal branching angle solution is

$$\cos \theta_0 = \frac{h_0^2 - h_1^2 - h_2^2}{2h_1h_2}, \quad \cos \theta_1 = \frac{h_1^2 - h_0^2 - h_2^2}{2h_0h_2}, \quad \cos \theta_2 = \frac{h_2^2 - h_0^2 - h_1^2}{2h_0h_1} \quad (1)$$

245 Note that our branching angles are defined differently than in Zamir (29, 30), so
246 these equations are equivalent but not identical. Recognizing our definitions are relative
247 to the parent rather than centerline extended from the parent, these expressions can be
248 straightforwardly translated into Zamir's solutions by subtracting our angles θ_1 and θ_2
249 from π . Moreover, we use the conventional counter-clockwise direction to define the
250 angles so that the trigonometric functions have consistent signs.

251 Notice that the branching angle solution for the stationary case does not exist
252 when the right side of the above expressions are not in the interval [-1,1]. For instance,
253 when $h_0 = 2.1$ and $h_1 = h_2 = 1$, then $\cos \theta_0 = 1.21$ and θ_0 is not defined. Values
254 outside of the allowed interval occur frequently when substituting in values from real
255 vasculature, so these equations should not be blindly applied and used without
256 considering the allowed regions and intervals. Moreover, there are cases for which an
257 optimal branching solution can be computed from the above equations, but the resulting

258 branching junction does not lie inside the triangle defined by the fixed vessel endpoints.
259 In this case, the computed optimum does not correspond to the true optimum, which
260 actually occurs at one of the fixed vessel endpoints (i.e., the vertices of the triangle).
261 Indeed, for both of these cases where the stationary solution either cannot be computed
262 or the computed answer lies outside the pre-defined triangle, the optimal solution is
263 actually attained at one of the singularity points, i.e. the vertices V_i .

264 Based on these observations, we find the conditions on the cost parameters and
265 the geometry of the fixed endpoints that correspond to degenerate branching solutions.
266 For example, when the cost per one vessel exceeds the total cost by the other vessels
267 ($h_i \geq h_j + h_k$), then the optimal branching occurs at the unshared end point of the
268 vessel i (V_i) to eradicate this particularly costly vessel. On the other hand, when the
269 solution θ_i defined by (1) is less than the angle $V_j V_i V_k$ (i. e. $\cos \theta_i > \cos V_j V_i V_k$), which we
270 refer to as the triangle condition, then the branching junction collapses onto the vertex
271 V_i . The details of the proof are given in the Appendix C.

272 These degeneracies are not specified in previous work (29, 30, 33) because
273 vessels are assumed to have volume flow rates that are proportional to r^3 . With this
274 presumption and by the conservation of volume flow rate across each branching
275 junction, those studies assume a strict relationship between radius of the parent and
276 daughter vessels (Generalized Murray's law: $r_0^d = r_1^d + r_2^d$, where $d \in [2,3]$ (32)) that
277 helps to avoid the degeneracy (Text S1). Moreover, previous work does not explicitly
278 consider cases in which the branching angle solution cannot satisfy the triangle
279 conditions defined above. Importantly, we find that these ignored cases and conditions

280 correspond to the vast majority of values calculated from empirical branching vessels
281 (Fig S2).

282 **2.3. Power-cost optimization for a single branching junction (PC-0)**

283 Another biological principle and property to optimize is the power loss to pump blood
284 from the heart to the capillaries. This principle is tantamount to minimizing the total
285 power for circulating blood or the total power lost that represents additional power
286 beyond what is used to move the blood. In this way, as much of the additional power as
287 possible is then redistributed and devoted to other needs such as foraging and
288 reproduction (2, 5). Much of the power that is required to push blood through the parent
289 and daughter vessels is lost due to dissipation, especially in the smaller vessels that
290 dominate the numbers and energetics of the whole vascular network. We calculate the
291 power dissipated by a single vessel in terms of the volume flow rate of the blood (\dot{Q}) and
292 the impedance (Z) via the formula $P_{loss} = \dot{Q}^2 Z$ (26, 31, 49). To correctly compute the
293 total power loss of all vessels connected by a single branching junction—a parent and
294 daughter vessels, we must employ rules of fluid dynamics to combine impedances into
295 an equivalent impedance. This equivalent impedance must in turn be used in the cost
296 function for the power minimization (see below), and as we show, the correct version is
297 different than the simple linear addition rule used by Zamir for both structural (correctly)
298 and flow (incorrectly) constraints (29, 30).

299 For any collection of vessels, total volume flow rate \dot{Q}_{TOT} is defined by flow
300 through a single cross section that cuts through all vessels at the same branching level.
301 Equivalent impedance Z_{eq} for the collection of vessels is defined by $Z = \Delta p / \dot{Q}$, based

302 on fluid dynamics (analog to Ohm's Law), where Δp is the pressure difference across
303 the extreme endpoints through which blood flows in and out of the entire collections of
304 vessels. The total power loss for the collected vessels is then calculated from $P_{loss} =$
305 $\dot{Q}_{TOT}^2 Z_{eq}$, where all of this is based on standard rules of fluid dynamics.

306 For a single branching junction, the optimization of power loss is derived for the
307 case that there is a source with a constant rate of flow, \dot{Q} , entering the parent vessel.

308 Based on our power loss equation ($P_{loss} = \dot{Q}_{TOT}^2 Z_{eq} \propto Z_{eq}$), the power-cost
309 optimization is then equivalent to just minimizing the equivalent impedance Z_{eq} of the
310 branching junction. By following the direction of the flow, we calculate the equivalent
311 impedance by noting that vessels at the same level (i.e., sibling vessels) are in a
312 parallel configuration, whereas the vessels across levels (i.e., parent and daughter
313 vessels) are in a series configuration. Pressure drop across sibling vessels may be
314 asymmetric but to simplify the calculation of an equivalent impedance, we further posit
315 that the pressure of the daughter vessels is approximately the same, i.e., $\Delta p_1 = \Delta p_2 :=$
316 Δp_d . Representing total volume flow rate of the daughter vessels by $\dot{Q}_{d,TOT} := \dot{Q}_1 + \dot{Q}_2$
317 and equivalent impedance of the daughter vessels by $Z_{d,eq}$, we have $\Delta p_d / Z_{d,eq} =$
318 $\Delta p_1 / Z_1 + \Delta p_2 / Z_2$. Canceling the pressure terms gives $Z_{d,eq} = \left(\frac{1}{Z_1} + \frac{1}{Z_2} \right)^{-1}$. By invoking
319 conservation of fluid, we can combine this expression with the parent vessel in series to
320 obtain $Z_{eq} = Z_0 + \left(\frac{1}{Z_1} + \frac{1}{Z_2} \right)^{-1}$ for the equivalent impedance of all the vessels that
321 connect at a single branching junction.

322 Assuming smooth, Poiseuille flow, the impedance of a single vessel is given
 323 by $Z = \frac{8\mu l}{\pi r^4}$, where μ is the viscosity of the blood (23, 26, 49, 50). Thus, for each vessel
 324 we implement a cost function of the form hl , where h is the cost per length, i.e. $h \equiv \frac{8\mu}{\pi r^4} \propto$
 325 $\frac{1}{r^4}$. Putting all of this together to find a solution for the PC-0 optimization (power loss at a
 326 single branching junction), our goal is to find the position of the branching junction that
 327 minimizes

$$Z_{eq} = h_0 l_0 + \left(\frac{1}{h_1 l_1} + \frac{1}{h_2 l_2} \right)^{-1}$$

328 By numerically calculating Z_{eq} as a function of the junction point and by using high
 329 resolution in space, we generate heat maps that illustrate the behavior of Z_{eq} . These
 330 heat maps reveal that the *branching junction always collapses onto one of the*
 331 *vertices*—unshared vessel endpoints—for *any values* of vessel radii (Fig S3). Based on
 332 our numerical evidence, we show analytically that power loss and equivalent
 333 impedance, Z_{eq} , attain minima only at a vertex of our original triangle that is defined by
 334 the unshared endpoints of the vessel. The specific vertex at which the junction
 335 collapses is determined both by the vessel radii and the relative locations of the
 336 unshared endpoints of the vessels. The proof follows from two steps. First, we calculate
 337 the equivalent impedance at each vertex to see how specific cases of cost parameters
 338 (h_0, h_1, h_2) determine which vertex is the best location for the branching junction J .
 339 Second, we show that when the junction is located within the triangle, Z_{eq} is always
 340 greater than the minimum value of the impedances when the junction is at a specific
 341 vertex. Together, this proves that the minimum of Z_{eq} is attained at one of the vertices

342 (Appendix D). Therefore, the PC-0 optimization leads to a degenerate branching
343 geometry by completely eliminating the vessel that is most costly.

344 Thus, minimizing power loss at a single branching junction leads to no branching
345 at all throughout the entire cardiovascular network. This is unrealistic as branching is
346 the most noticeable and perhaps most important feature of the vascular system or any
347 resource-distribution network. Therefore, we consider how to modify the power-cost
348 minimization to attain more biologically realistic results that include vascular branching
349 and thus lead to predictions for the branching angles and vessel lengths. In the next
350 section, we describe how to adapt the power-minimization calculation to include larger
351 sections of the network that expand beyond a single branching junction to encompass
352 downstream vessels and branching junctions.

353 **2.4. Power-cost optimization beyond a single branching junction (PC-1)**

354 The solutions above thus lead to a single path that would prevent the vascular system
355 from distributing blood to all the downstream vessels, capillaries, and cells. To
356 overcome these problems, we include larger sections of the vascular network by
357 incorporating impedances of downstream vessels. To do this generically, we recognize
358 that downstream vessels are in series with each of the daughter vessels, so we can
359 represent the downstream impedance by adding constant terms c_1 and c_2 to the
360 impedance of the daughter vessels. Thus, the equivalent impedance of the bifurcation
361 becomes

$$\tilde{Z}_{eq} = Z_0 + \left(\frac{1}{Z_1 + c_1} + \frac{1}{Z_2 + c_2} \right)^{-1}$$

362 For the case of vessels above the capillaries, these constant terms represent the
363 impedance from all of the downstream vessels. For the capillary case, these constant
364 terms are still not zero, however, because they represent the minimum impedance of a
365 capillary, which is not allowed to be zero. We now investigate different geometries for a
366 single branching junction for which the downstream impedances c_1 and c_2 are constant.

367 We simplify this problem using a few general principles. First, when the
368 impedance of the parent vessel and the branching daughter vessels are matched, no
369 pulsatile reflections occur and the power loss at the bifurcation is minimized (26, 49).
370 Second, we assume the simple case that the siblings have identical impedances and
371 each sibling has the same number of downstream vessels. From these two
372 assumptions, we find that the equivalent downstream impedance is much larger than
373 single vessel impedances except for vessels close to the capillaries (Appendix E).

374 Because the number and small surface-areas of capillaries will again likely
375 dominate the power loss for the network, we solve the optimization problem when the
376 downstream impedances are large, i.e. $c_i \gg Z_i$. Consequently, we expand \tilde{Z}_{eq} as a
377 series to first order and obtain the following approximation:

$$\tilde{Z}_{eq} \sim Z_0 + \frac{c_2^2}{(c_1 + c_2)^2} Z_1 + \frac{c_1^2}{(c_1 + c_2)^2} Z_2 + \frac{c_1 c_2}{c_1 + c_2}$$

378 We note that the constant term $\frac{c_1 c_2}{c_1 + c_2}$ can be ignored because its derivative is zero and
379 hence does not influence the optimization. As a result, we want to find the location of
380 the branching junction that minimizes

$$h_0 l_0 + \frac{c_2^2}{(c_1 + c_2)^2} h_1 l_1 + \frac{c_1^2}{(c_1 + c_2)^2} h_2 l_2$$

381 The coefficients $\frac{c_2^2}{(c_1+c_2)^2}$ and $\frac{c_1^2}{(c_1+c_2)^2}$ are always less than 1, so the cost per length for the
 382 daughter vessels are diminished by these rescaling constants, thus reducing the
 383 likelihood the solution will collapse onto a daughter vessel endpoint. Defining the non-
 384 dimensionalized ratio $k := c_1/c_2$, the optimization function becomes

$$H := h_0 l_0 + \frac{1}{(k+1)^2} h_1 l_1 + \frac{k^2}{(k+1)^2} h_2 l_2$$

385 This further implies that the cost of the daughter vessel with the larger downstream
 386 impedance is diminished less than the cost of the other daughter vessel. This pushes
 387 the optimal branching junction towards the daughter vessel with smaller downstream
 388 impedance.

389 The new optimization function for power loss above (i.e. PC-1) has the same
 390 form as the cost function for the material-cost optimizations in section 2.2, except that
 391 the costs per length for daughter vessels are rescaled by terms that depend on k . We
 392 therefore simplify the notation and define $\tilde{h}_0 = h_0$, $\tilde{h}_1 = \frac{1}{(k+1)^2} h_1$, $\tilde{h}_2 = \frac{k^2}{(k+1)^2} h_2$. With
 393 these definitions for \tilde{h}_i , we can immediately use our results for Eq. (1) to obtain the
 394 stationary solution for which the branching junction occurs inside the triangle of the
 395 unshared end points.

396 As for Eq. 1 and the material-cost optimizations, the stationary solution does not
 397 exist or does not provide the minimum and the degenerate solution occurs at vertex V_i

398 for the following cases: 1) $\tilde{h}_i \geq \tilde{h}_j + \tilde{h}_k$ or 2) $\cos \theta_i = \frac{\tilde{h}_i^2 - \tilde{h}_j^2 - \tilde{h}_k^2}{2\tilde{h}_j\tilde{h}_k} > \cos V_j V_i V_k$. These
399 two conditions correspond to six inequalities in terms of $k (= c_1/c_2)$ if we take all
400 combination of i, j , and k . Solving these, we obtain the values of k that result in solutions
401 within the triangle versus those that collapse on an unshared endpoint at a vertex.
402 Mapping these values into the $c_1 c_2$ -plane yields predictable lines that separate the plane
403 into regions classified as non-degenerate (collapse onto a vertex) or degenerate
404 (junction within the triangle) solutions. Indeed, by using approximations to solve the
405 above limiting case ($\frac{Z_i}{c_i} \ll 1$), we predict the full solution space. The validity of our
406 approximate solutions for this PC-1 optimization problem is further explored in the
407 Results section by comparing with numerical solutions.

408 **2.5. Expanding from local to global constraints for the random placement of
409 branching junctions**

410 The above optimization schemes are based on the local consideration of branching
411 junctions: at each branching the unshared end points (V_i) are fixed and the branching
412 junction (J) is attained within the triangle of these end points (Fig 1c, Fig A1). To explore
413 the effects of the size of the constraint region, we now consider relaxing the locality
414 assumption to various degrees between fully local to fully global.

415 We simulate the branching network by randomly placing branching junctions
416 within regional constraints that range from local to global. For all the simulations, the
417 hierarchical ordering of vessels, the location of the terminal tips, and most upstream
418 branching nodes (i.e., the source) are the same as in the empirical data. We repeated

419 each simulation type 100 times to get the average behavior of network characteristics.
420 All these different simulation types are illustrated with an example network that has 3
421 branching levels (Fig 2).

422 For the fully local case, we randomly place a branching junction inside each
423 triangle of unshared end points of three connected vessels, corresponding to the same
424 size of spatial constraint as in our optimizations above (Fig 2). For the fully global case,
425 we only require that the branching junctions are randomly positioned within a minimum
426 sphere that contains all nodes from the real data (Fig 2) and that the network terminates
427 at the appropriate (most extreme upstream and downstream) endpoints in the network.

428 For intermediate degrees of regional constraint between the fully local case and
429 fully global cases, we consider two possibilities. These intermediate states are
430 constructed such that they involve sequential updates of the branching junction. The
431 first intermediate randomly branching network simulation (intermediate 1) starts by
432 randomly positioning a branching junction within the local triangle corresponding to the
433 most upstream vessel (i.e., source) of the network and the endpoints of its two daughter
434 vessels. Based on the new location of this branching junction, the endpoints of the
435 daughter vessels are then updated and used to define new triangles in the next step in
436 which the daughters become the parents. The simulation continues this updating
437 process by working down through the network until it reaches the terminal tips of the
438 network (Fig 2, Fig S4). Notably, this simulation leads to branching junctions that are
439 approximately confined to the plane. The other intermediate randomly branching
440 network (intermediate 2) starts with the terminal tips (most downstream vessels of the
441 network) and builds backwards to the first branching node (i.e., the source). We assign

442 the position of each branching junction by creating a spherical boundary around the
443 fixed two downstream end points (i.e. V_1 , V_2 , Fig 1c, Fig A1) such that the center of the
444 sphere is at the midpoint of V_1V_2 and the sphere has a radius of the length $|V_1V_2|$. We
445 then randomly position the branching junction at a point that can occur anywhere within
446 the boundary of this three-dimensional sphere. Thus, for this simulation each branching
447 junction may not fall within the plane defined by the vessel endpoints, as it does for the
448 first simulation for intermediately-constrained random branching. For this case, the
449 upstream endpoint (i.e., V_0) does not affect the location of the branching junction,
450 reducing the degree of locality compared with the other simulation for an intermediate
451 constraint.

452 **3. Results**

453 We begin this section with empirical data for asymmetry in the vascular branching of
454 mouse lung and human head and torso. Following this, we present the results of our
455 local optimization schemes. Next, we present results for our exploration of different
456 regional constraints for randomly-placed branching junctions and compare these results
457 with empirical data. Finally, we provide statistical analysis of different optimization
458 schemes and random-branching results as compared with the empirical data. This
459 comparison enables us to quantitatively investigate how well our predictions match the
460 empirical measurements of asymmetry in vasculature, and thus, to characterize whether
461 different optimizations or random processes might underlie the systematic patterns we
462 observe.

463 **3.1. Analysis of asymmetry patterns in vascular data**

464 To characterize the branching asymmetry of the vascular structure, we calculate
465 asymmetry ratios between siblings. In particular, the asymmetry ratios for radius and
466 length are $\lambda_r = r_1/r_2$ and $\lambda_l = l_1/l_2$, respectively, where the value of the sibling with the
467 larger radius or length is always chosen to be in the denominator ($r_1 \leq r_2, l_1 \leq l_2$) (20,
468 26, 51). Thus, a ratio of 1 indicates perfect symmetry, whereas smaller values indicate
469 more asymmetrical branching. We further provide a similar measure to quantify local
470 asymmetry in sibling branching angles as $\lambda_\theta = \theta_1/\theta_2$ again with $\theta_1 \leq \theta_2$ (Fig 1c).

471 It is easy to see that asymmetry in vessel lengths is related to asymmetry in
472 branching angles. When the downstream ends of the daughter vessels are equidistant
473 from both the upstream and downstream ends of the parent vessel, siblings have
474 identical length and branching angles, resulting in symmetry $\lambda_l = \lambda_\theta = 1$. However, if
475 daughter vessels are not equidistant from the upstream end, even symmetric sibling
476 lengths can result in asymmetric branching angles or vice versa. Therefore, the value
477 of λ_θ represents a combination of the asymmetry in lengths and the asymmetry of the
478 alignment of daughter vessel end points.

479 After executing Angicart on high-quality tomographic images, we quantified the
480 extent to which the analyzed networks are asymmetric by plotting the frequency
481 distributions of λ_r , λ_l , and λ_θ (Fig 3a, b). Even though asymmetric radius branching
482 exists, data for both mouse and human show distributions of λ_r that are skewed
483 towards 1, meaning that the radius ratio is skewed towards perfect symmetry. In
484 contrast, the length asymmetry ratio (λ_l) is distributed almost uniformly, suggesting a
485 high degree of asymmetry in sibling lengths. The frequency distribution of branching
486 angle asymmetry (λ_θ) is biased towards the right, corresponding to perfect symmetry in

487 both networks and similar to results for asymmetry in radii (statistical calculations are
488 given in section 3.5). That is, a parent vessel tends to branch into sibling vessels that
489 are separated by equal branching angles. Intriguingly, the similarity of the pattern
490 observed in radius asymmetry might suggest a correlation between the radius and the
491 branching angle, providing motivation to investigate how branching angle depends on
492 radius.

493 In addition to the asymmetry ratios explored above, we plot the histogram for the
494 raw data on branching angles. Human and mouse networks show similar patterns, so
495 we combine data for these two networks in our histogram plot (Fig 3c). Analyzing the
496 branching angle between the sibling vessels (θ_0) and the branching angle between the
497 parent and daughter vessels (θ_1 and θ_2) separately, we find unimodal distributions that
498 peak at 1.51 and 2.21 radians, respectively. This shows that planar branching (52, 53)
499 with orthogonal daughter vessels is frequent across the networks. Individual branching
500 angle plots for mouse and human networks are given in Fig S5a, b.

501 Altogether, these network-level patterns for vessel radius, length, and branching
502 angles hold across 18 different human subjects, different species (human and mouse),
503 and different tissues (head and torso versus lung). Moreover, the radius and length
504 asymmetries are consistent with findings in plants (41-43). These results suggest that
505 very general and ubiquitous selection pressures and developmental processes may
506 shape the architecture of the vascular system across taxa, from humans to mice to
507 plants, as well as across tissues, from lungs to head and torso.

508 **3.2. Optimal branching patterns for material-cost optimization**

509 In this section, we introduce the MC optimization results that include surface-area (MC-
510 SA) and volume (MC-V) constraints. Here, we only focus on non-degenerate branching
511 solutions—solutions that do not collapse to a vertex—and compare those with real data.
512 The fraction of the non-degenerate and degenerate cases is provided in the Fig S6.

513 **3.2.1. Network-level comparison**

514 Taking the values for the radii and vessel endpoint information from our real human and
515 mouse vascular networks, we use the solution provided above in section 2.2 (Eq. 1) to
516 compute the optimal branching angle and length asymmetry at each branching junction.
517 To compare predicted values to the real network structures presented in section 3.1, we
518 plot the distributions of λ_l and λ_θ as well as the raw branching angle distributions for θ_0
519 and θ_1 & θ_2 . We find that all these properties are visually consistent across both
520 networks and for both volume and surface-area constraints.

521 In particular, distributions of optimal λ_l are close to uniform, whereas optimal λ_θ
522 distributions are skewed towards perfect symmetry (Fig 4a, b). Both of these match the
523 general patterns of asymmetry in branching observed in Fig 3. However, the degree of
524 skewness in optimal λ_θ is sharper than the real λ_θ distributions, especially for the MC-
525 SA. The statistical analysis of all these plots (including mean, median, skewness) are
526 presented in section 3.5.

527 Next, we plot optimal θ_0 and θ_1 & θ_2 histograms for the combined datasets (Fig
528 5). We observe that optimal calculations yield unimodal distributions as in histograms of
529 the real data. Optimal θ_0 shows a mode around 1.80 radians, hence the optimal
530 calculations are shifted towards larger values compared to the actual θ_0 distribution that

531 have a mode at 1.51 radians. In contrast, the peak for the uniform distribution $\theta_1 \& \theta_2$ at
532 2.24 radians almost matches the actual peak at 2.21 radians. The separate figures for
533 human and mouse networks for each constraint are given in the Fig S5. The full
534 statistical analysis of branching angle histograms for the individual networks and the
535 combined datasets are provided in the Table S1.

536 **3.2.2 Junction-level comparison**

537 The previous section compares the network-level patterns of the optimal calculations
538 and the empirical data. Here, we provide comparisons at local branching junctions for
539 the material-cost optimizations. To view this, we plot actual versus optimal branching
540 angles and calculate the Pearson correlation coefficient, which would be 1 if our
541 predictions were always perfect. From the plots of branching angle for MC-V (Fig 6) and
542 MC-SA (Fig S7) optimizations, we find that the predictions and the empirical data are
543 weakly correlated (p -values <0.05). Moreover, we see that the volume constraint yields
544 better agreement with data than the surface-area constraint at the junction-level
545 comparison. However, the correlation coefficients for both constraints indicate that the
546 predicted optimal branching angles are a weak predictor of the actual branching angles
547 at the local-junction level. Consequently, it seems our theory needs further refinement
548 or replacement.

549 **3.3. Analytical Solutions for Power-cost optimization Beyond Single Branching**
550 **(PC-1)**

551 Now, we introduce the results for the solution of the PC-1 optimization. As described in
552 section 2.4, we derived the approximate solution by considering a limiting case of the

553 downstream impedances c_1 and c_2 . With this method our solution predicts regions in the
554 c_1c_2 -plane separated by lines over most of the range of values. The regions in the c_1c_2 -
555 plane correspond to combinations of values that lead to branching geometries that are
556 categorized as follows: collapse to daughter end point, collapse to parent end point, or
557 no-collapse (i.e., a non-degenerate branching point).

558 Using the vessel end-point and radius information from the real data, we predict
559 the linear equations that form the boundaries between these regions, and we label them
560 according to the categories of solution described above (Fig 7). As a further check, we
561 compute numerical solutions at each discretized point in the c_1c_2 -plane and mark
562 different categories of solution by different colors. We examine two examples,
563 corresponding to symmetric (Fig 7a, b) and asymmetric (Fig 7c, d) parameter values.
564 Both show that our approximate analytical solution matches the numerical solution
565 extremely well. On closer inspection, it is clear that the different regions and categories
566 are not separated via purely linear functions across the entire plane, but instead the
567 boundaries are curved for small values of c_1 and c_2 (Fig 7b, d). This result reveals a
568 mismatch between the analytical and numerical solution at the smallest scales, i.e.
569 vessels close to the capillaries, which is exactly where our solutions should fail based
570 on the limits of our approximation scheme.

571 **3.4. Network-level results of randomly branching networks with local to global
572 constraints**

573 Lastly, we compare our empirical results for network-level characteristics of branching
574 angles and length asymmetries to results from simulated randomly branching networks

575 with local to global constraints. Because mouse and human networks yield similar
576 results, we only present results for the mouse in the main text. Random simulation
577 results for the human subjects are given in Fig S8.

578 As in the empirical data, random simulations with local to intermediate
579 constraints yield uniform distributions for asymmetric length ratio (λ_l), whereas the
580 branching-angle asymmetry ratio (λ_θ) is skewed towards symmetry (Fig 2). In contrast,
581 the fully global constraint generates branching networks that are skewed towards
582 symmetry for both λ_l and λ_θ , inconsistent with empirical data (Fig 2). Further statistical
583 comparisons with empirical data and optimal branching results are presented in the next
584 section.

585 **3.5. Comparison of optimal branching, random branching, and empirical data**

586 To provide a rigorous comparison across different material-cost optimizations (surface-
587 area and volume) and spatial constraints (local to global) with the empirical data, we
588 compute the statistical properties— mean, standard deviation (SD), skewness and
589 standard error for each—of the resulting asymmetry distributions in Table 1.
590 Additionally, we use the Kullback-Leibler divergence measure (KL) to quantify the
591 distance between the empirical asymmetry distributions and the optimization or random-
592 simulation asymmetry distributions. We determine p-values by performing bootstrap
593 samples up to half the size of the real data (54). By definition, a p-value is equal to 1.00
594 for a comparison of the real data with itself because that implies an exact match in the
595 distributions.

596 **Table 1. Statistical comparison of material-cost optimizations and spatial
597 constraints with empirical data.**

		length asymmetry (λ_l)				branching angle asymmetry (λ_θ)			
		Mean± SE	SD± SE	Skewness± SE	KL p-value	Mean± SE	SD± SE	Skewness± SE	KL p-value
real network	mouse lung	0.53± 0.00	0.25± 0.00	0.13± 0.00	1.00	0.76± 0.00	0.16± 0.000	-0.43± 0.00	1.00
material-cost optimizations	surface-area	0.54± 0.00	0.27± 0.00	-0.07± 0.00	0.01	0.82± 0.00	0.16± 0.00	-1.28± 0.00	0.00
	volume	0.54± 0.00	0.27± 0.00	-0.09± 0.00	0.00	0.74± 0.0	0.20± 0.00	-0.79± 0.00	0.01
randomly simulated networks	local	0.56± 0.01	0.25± 0.00	-0.10± 0.04	0.61	0.65± 0.01	0.24± 0.00	-0.43± 0.04	0.26
	intermediate 1	0.56± 0.01	0.25± 0.00	-0.09± 0.05	0.59	0.68± 0.01	0.22± 0.00	-0.54± 0.07	0.64
	intermediate 2	0.57± 0.01	0.24± 0.00	-0.12± 0.05	0.11	0.63± 0.01	0.23± 0.00	-0.38± 0.06	0.00
	global	0.76± 0.01	0.22± 0.01	-0.85± 0.07	0.00	0.71± 0.01	0.26± 0.01	-0.65± 0.06	0.00
real network	human head and torso	0.46± 0.00	0.29± 0.00	0.22± 0.00	1.00	0.75± 0.00	0.19± 0.00	-1.07± 0.00	1.00
material-cost optimizations	surface-area	0.46± 0.00	0.29± 0.00	0.14± 0.00	0.64	0.85± 0.00	0.15± 0.00	-1.71± 0.00	0.00
	volume	0.48± 0.00	0.28± 0.00	0.10± 0.00	0.00	0.78± 0.00	0.19± 0.00	-1.01± 0.00	0.00
randomly simulated networks	local	0.54± 0.01	0.27± 0.00	-0.07± 0.03	0.00	0.63± 0.01	0.28± 0.00	-0.50± 0.03	0.00
	intermediate 1	0.53± 0.01	0.26± 0.00	-0.01± 0.05	0.00	0.66± 0.01	0.26± 0.00	-0.64± 0.04	0.03
	intermediate 2	0.59± 0.01	0.23± 0.00	-0.22± 0.05	0.00	0.62± 0.01	0.23± 0.00	-0.34± 0.05	0.00
	global	0.76± 0.01	0.22± 0.00	-0.81± 0.06	0.00	0.70± 0.01	0.26± 0.01	-0.60± 0.05	0.00

598

599 There are several conclusions based on these results. First, the random
600 branching simulations that are globally constrained do not produce results that are
601 statistically similar with mouse lung or human head and torso in terms of length
602 asymmetry. In addition, the second intermediate constraint—spheres are used to
603 determine the branching locations, Fig 2—on random branching poorly matches with

604 real data in terms of both length and branching angle asymmetries for the human head
605 and torso network.

606 Except for the global constraint, results for the mouse-lung network reveal that
607 the random branching simulations perform as well as the material-cost optimizations in
608 terms of the general characteristics (i.e. the first few moments—mean, SD, skewness)
609 of the distributions. In contrast, for the human head and torso, the material-cost
610 optimizations yield overall better agreement with the real data than the random
611 simulations, especially for the length asymmetry. This finding is consistent with the KL
612 significance test. Based on the KL p-values, we observe that all of the random
613 branching simulations do not do a good job of matching the real data for human
614 networks. However, it suggests that vascular branching derived from MC-SA do
615 reasonably well at recreating length asymmetry patterns that are similar to real human
616 data. In contrast, the mouse lung compares more favorably with the random-branching
617 simulations at local and intermediate scales than it does with the material-cost
618 optimizations (Table 1).

619 **4. Discussion**

620 By performing a high-quality analysis of angiographic images from mouse lung and
621 human head and torso via the new software Angicart (28, 39), we identified systematic
622 patterns in the branching asymmetry of the vascular system. Specifically, the radii and
623 branching angles of sibling vessels tend to be symmetric, while the lengths of sibling
624 vessels tend to be asymmetric. Such systematic patterns in asymmetry suggest there
625 may exist underlying biological principles that could vary in selection strength and

626 across spatial scales yet effectively constrain the structure of the vascular system. In
627 this study, we focus on MC (material-cost) and PC (power-cost) optimizations that have
628 long been postulated as evolutionary principles that play a critical role in the formation
629 of the vascular system (29, 30, 32, 33). We provide a consistent and robust framework
630 for studying these optimization principles and for discovering possible associations with
631 the asymmetry patterns observed in the real data.

632 We first examined the local optimization and for the first time presented full
633 solutions for the material-cost optimization that uncovers misidentified solutions—
634 calculations from formula yield answers that are not optimal—from previous studies. We
635 have further shown that solutions predicted from MC optimizations match the network-
636 level asymmetry patterns for lengths and branching angles observed in the real data.
637 Following this, we built a PC optimization scheme that is consistent with the basic rules
638 of fluid dynamics and corrects inconsistencies about fluid mechanics—incorrectly
639 summing impedances in series and parallel—from previous work. Based on the correct
640 fluid mechanics relationship, we find for single branching junctions that one vessel is
641 always sufficiently costly that it is better to completely eliminate it and have no
642 branching at all. Of course, repeating this solution at each junction throughout the
643 network will result in a single vessel for the entire cardiovascular network, which is
644 unrealistic because it violates the need to efficiently distribute blood throughout the body
645 (14, 15, 26, 31, 32). Consequently, based on our new analysis, we conclude that
646 optimization of flow and power loss at a single branching junction (i.e. PC-0
647 optimization) will always lead to the elimination of branching and thus lead to

648 meaningless results for efforts trying to predict angles and lengths of vessels in
649 branching networks.

650 In an attempt to connect vascular branching asymmetry with the efficient flow
651 mechanisms, we included multiple downstream vessels and branching junctions as part
652 of the power-cost optimization (i.e. PC-1 optimization) to determine the optimal
653 placement of each individual branching junction. This in turn indicates the need to
654 consider constraints beyond just the local spatial and branching junction scale. Although
655 this is additional work, it has the advantage that capillaries are at a uniform pressure so
656 that the full downstream vascular tree below each daughter vessel has a symmetric
657 pressure drop, thus simplifying the optimization problem. Alternatively, the model could
658 be improved by allowing asymmetric pressure drops across sibling vessels that could
659 lead to plausible (i.e., non-degenerate) solutions even when locally optimizing the flow.
660 However, determining these pressure drops would also require considering effects from
661 multiple branching junctions when calculating the placement of a single branching
662 junction. Furthermore, our results from these more intermediate-scale calculations
663 reveal that plausible explanations and predictions for branching angles and length
664 asymmetry can be obtained by incorporating vessels beyond a single branching
665 junction. Thus, from any perspective, we argue that local-scale optimization principles
666 and constraints are insufficient to understand and predict asymmetric branching
667 patterns, in strong contrast to many previous result for symmetric branching that can be
668 fully treated at the local scale or a single branching junction.

669 There is no a priori reason that evolutionary constraints should only apply at local
670 spatial scales. Thus, to investigate the role of spatial constraints on the vascular

671 structure, we considered random simulations of the branching network by varying the
672 constraints from local to global, including two types of constraints at intermediate
673 scales. We find that the global constraint performs poorly, whereas the intermediate or
674 local constraints provide reasonable matches to the network-level observations from
675 real data. Here, the intermediate constraints are especially important to consider
676 because they incorporate the downstream impedance as in our improved power-cost
677 optimization scheme.

678 Although some optimization results match empirical data at the network-level, the
679 junction-level comparisons show that a single, local constraint is likely not the only
680 driving factor for the vascular structure, or rather may not be strictly or strongly applied
681 at that most local of scales. In addition, the fact that the power-cost optimization scheme
682 does not lead to any branching suggests that local constraints are not sufficient. We
683 enlarged the scale of spatial constraint and number of branching junctions involved in
684 the optimization to incorporate more information.

685 We have characterized optimal branching patterns by rigorously deriving results
686 based on commonly-considered evolutionary principles at a local spatial scale and by
687 enforcing constraints on random branching at scales that range from local to global.
688 Results from the global scale yield asymmetric branching patterns that strongly disagree
689 with patterns in the real data, whereas optimizations or constraints at intermediate or
690 local spatial scales are fairly consistent with the direction of the real asymmetric
691 branching patterns.

692 More specifically, statistical analysis that compares network-level asymmetry
693 from empirical data to optimal predictions and randomized results show that random
694 simulations and material-cost optimizations capture important features of the vascular
695 branching for the mouse-lung network. For the human head and torso, we find that only
696 material-cost optimizations succeed at capturing the dominant features of asymmetry in
697 vascular branching. This difference may arise because the human head and torso
698 represent vessels of larger sizes that must spread from the heart to the rest of the body
699 and thus may be more programmed to follow a defined branching pattern. In contrast,
700 the smaller-sized vessels in the lung may be filling space but with a structure that
701 requires weaker constraints on the patterns of asymmetry in vascular branching. Our
702 results are intriguing because an intermediate spatial scale has been found to be the
703 correct spatial scale for recreating pervasive patterns founds in urban studies on cities
704 (55).

705 Taken together, our findings suggest that combinations of biological principles
706 that are applied at the intermediate- and local-level could eventually lead to the
707 systematic patterns for branching angles and length asymmetry observed in real data.
708 We infer that physical constraints, evolution, and optimization principles may play a
709 major role in determining the vascular structure but that this conclusion likely depends
710 more sensitively on the spatial scale and number of branching junctions involved, the
711 size of the vessels being considered, and the tissue type than previously recognized. As
712 a result, our work suggests further exploration of optimal branching at local and
713 intermediate spatial scales in a way that combines and integrates multiple optimization
714 principles.

715 **Acknowledgments**

716 We thank Kristina Bostrom for providing the micro-CT images of mouse lungs used in
717 this study, and J. Paul Finn and Derek Lohan for providing MRI images of human head
718 and torso used in this study. We thank David Hunt for stimulating discussions for this
719 study and comments on the manuscript. We also thank Kathryn Burch, Maya Josyula,
720 Edward Hu, and Quinten Lepak for their preliminary work on this topic.

721 **Figure Captions**

722 **Fig 1. Cardiovascular data and schematic illustration of vascular branching (a)**
723 Mouse lung micro-CT images processed by Angicart. **(b)** Human head and torso MRI
724 images processed by Angicart. **(c)** Schematic illustration of the asymmetric branching
725 geometry and labeling. Parent vessel with radius r_0 and length l_0 branches into two
726 daughter vessels with radius r_i and length l_i with subscript $i = 1$ or 2 . Branching angles
727 are defined by the angle between the centerlines of the vessel pairs, where subscripts
728 are determined by the non-adjacent vessel.

729 **Fig 2. Comparison of real data for vascular networks versus random simulations**
730 **of branching junctions.** The real and simulated networks (via local to global spatial
731 constraints) are separated by different rows. A schematic small network is given to
732 describe how different simulations are performed. The vessels and the fixed end points
733 of the real branching network are represented in red. Vessels that result from random
734 branching simulations are in black. The healthy mouse lung network and the simulated
735 mouse lung networks are shown within a minimum spherical boundary that contains all
736 branching data from the real network. Here, the red nodes for each figure correspond to

737 the real data, whereas the black nodes correspond to the simulated data. Note that the
738 terminal tips and the most upstream node (i.e., the source) are determined from real
739 data and fixed throughout all simulations. The resulting asymmetry ratio distributions for
740 length and branching angles are provided for the real network and for each of the
741 simulations. The statistical comparisons of random branching simulations with empirical
742 data are given in section 3.5.

743 **Fig 3. Histograms or frequency distributions of the asymmetry ratios for radius**
744 **(λ_r), length (λ_l), and branching angles (λ_θ) of vascular networks. (a)** mouse lung
745 (1 individual) and **(b)** human head and torso (18 individuals). Note that radius and
746 branching angle asymmetry ratios are both skewed towards perfect symmetry, whereas
747 the length asymmetry ratio shows no skew and reveals much more asymmetry. **(c)**
748 Histograms of branching angles for combined data of human and mouse networks
749 appear to be unimodal both for θ_0 and for θ_1 & θ_2 with peaks at 1.51 and 2.21 radians,
750 respectively.

751 **Fig 4. Histograms or frequency distributions of optimal asymmetry ratios for**
752 **length (λ_l) and branching angle (λ_θ) derived from material-cost optimization.**
753 Surface-area (MC-SA) results are shown as solid lines and volume (MC-V) results are
754 shown as dashed lines for **(a)** mouse lung and **(b)** human head and torso.

755 **Fig 5. Histogram of optimal branching angles for combined data of human and**
756 **mouse networks for material-cost optimizations.** All histograms appear to have
757 unimodal characteristics both for θ_0 and for θ_1 & θ_2 with respective peaks at **(a)** 1.80
758 and 2.24 for the surface-area constraint and **(b)** 1.80 and 2.24 for the volume constraint.

759 **Fig 6. Junction-level comparison of optimal versus actual branching angles for**
760 **the volume constraint of material-cost optimizations (MC-V). (a)** mouse lung and
761 **(b)** human head and torso. The Pearson correlation coefficients and p-values are
762 calculated for each plot.

763 **Fig 7. Comparison of approximate solutions with numerical solutions for the PC-1**
764 **(power-cost optimization beyond single branching).** Approximate solutions define
765 linear boundaries on the $c_1 c_2$ -plane between different categories of the solution space:
766 collapse to daughter end point, collapse to parent end point, and no-collapse. The
767 different categories calculated from numerical simulation are marked by different colors
768 as indicated in the figure. **(a)** An example of symmetric branching in vessel radius with
769 parameter values: $|V_0 V_1| = |V_0 V_2| = |V_1 V_2| = 1$, $r_0 = 1.20$, $r_1 = 1$, and $r_2 = 1$, where c_1
770 and c_2 take values in the range $[0,20]$. **(b)** Zoomed version of (a) into the plane $[0,2] \times$
771 $[0,2]$ with the same resolution as in (a). **(c)** An example of asymmetric branching in
772 vessel radius with parameter values: $|V_0 V_1| = 0.8$, $|V_0 V_2| = |V_1 V_2| = 1$, $r_0 = 1.1$, $r_1 = 0.85$,
773 and $r_2 = 1$, where c_1 and c_2 take values in the range $[0,20]$. **(d)** Zoomed version of (c)
774 into the plane $[0,2] \times [0,2]$ with the same resolution as in (c).

775 **References**

- 776 1. Brown JH, Gillooly JF, Allen AP, Savage VM, West GB. Toward a Metabolic
777 Theory of Ecology. *Ecol.* 2004;85(7):1771-89.
778 2. Brown JH, West GB, editors. *Scaling in Biology*. New York: Oxford University
779 Press; 2000.
780 3. Savage VM, Allen AP, Gillooly JF, Herman AB, Brown JH, West GB. Scaling of
781 Number, Size, and Metabolic Rate of Cells with Body Size in Mammals. *Proc Natl Acad
782 Sci.* 2007;104(11):4718-23.
783 4. Savage VM, Deeds EJ, Fontana W. Sizing Up Allometric Scaling Theory. *PLoS
784 Comp Biol.* 2008;4(9):e1000171.
785 5. West GB, Brown JH, Enquist BJ. A General Model for the Origin of Allometric
786 Scaling Laws in Biology. *Science.* 1997;276:122-6.
787 6. Kleiber M. Body size and metabolic rate. *Physiological Reviews.* 1947;27(4):511-
788 41.
789 7. Kleiber M. *The Fire of Life: An Introduction to Animal Energetics*. New York:
790 Wiley; 1961.
791 8. Hemmingsen AM. Energy metabolism as related to body size and respiratory
792 surfaces, and its evolution. *Reports of the Steno Memorial Hospital and Nordisk Insulin
793 Laboratorium.* 1960;9:1-110.
794 9. Kolokotrones T, Deeds EJ, Savage VM, Fontana W. Curvature in metabolic
795 scaling. *Nature* 2010;464(7289):753-6.
796 10. Savage VM, Gillooly JF, Woodruff WH, West GB, Allen AP, Enquist BJ, et al. The
797 predominance of quarter-power scaling in biology. *Functional Ecology.* 2004;18:257-82.
798 11. Dodds PS, Rothman DH, Weitz JS. Re-examination of the ``3/4-law'' of
799 Metabolism. *J Theor Biol.* 2001;209:9-27.
800 12. Clarke A, Rothery P, Isaac NJ. Scaling of basal metabolic rate with body mass
801 and temperature in mammals. *Journal of Animal Ecology.* 2010;79(3):610-9.
802 13. Mori S, Yamaji K, Ishida A, Prokushkin SG, Masyagina OV, Hagihara A, et al.
803 Mixed-power scaling of whole-plant respiration from seedlings to giant trees.
804 *Proceedings of the National Academy of Sciences.* 2010;107(4):1447-51.
805 14. Banavar JR, Maritan A, Rinaldo A. Size and Form in Efficient Transportation
806 Networks. *Nature.* 1999;399:130-2.
807 15. Banavar JR, Cooke TJ, Rinaldo A, Maritan A. Form, function, and evolution of
808 living organisms. *Proceedings of the National Academy of Sciences.* 2014;111(9):3332-
809 7.
810 16. Dodds PS. Optimal form of branching supply and collection networks. *Physical
811 review letters.* 2010;104(4):048702.
812 17. Huo Y, Kassab GS. Intraspecific scaling laws of vascular trees. *Journal of The
813 Royal Society Interface.* 2012;9(66):190-200.
814 18. West GB, Brown JH, Enquist BJ. The fourth dimension of life: Fractal geometry
815 and allometric scaling of organisms. *Science.* 1999;284(#5420):1677-9.
816 19. Schroeder MF. *Fractals, chaos, power laws*. New York: W.H. Freeman and
817 Company; 1991.
818 20. Zamir M. On Fractal Properties of Arterial Trees. *J Theor Biol.* 1999;197(4):517-
819 26.

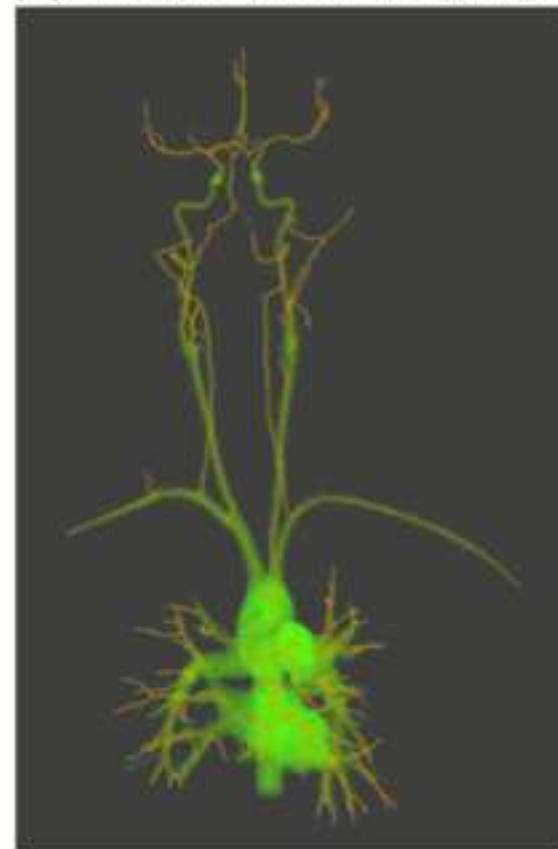
- 820 21. Allmen EI, Sperry JS, Smith DD, Savage VM, Enquist BJ, Reich PB, et al. A
821 species-level model for metabolic scaling of trees II. Testing in a ring- and diffuse-
822 porous species. *Functional Ecology*. 2012;doi: 10.1111/j.365-2435.012.02021.x.
- 823 22. Zamir M. Vascular system of the human heart: some branching and scaling
824 issues. *Scaling in Biology* Oxford University Press, Oxford. 2000:129-44.
- 825 23. Caro CG, Pedley TJ, Schroter RC, Seed WA. *The Mechanics of Circulation*.
826 Oxford, UK: Oxford University Press; 1978.
- 827 24. Kalsho G, Kassab GS. Bifurcation asymmetry of the porcine coronary
828 vasculature and its implications on coronary flow heterogeneity. *American Journal of*
829 *Physiology-Heart and Circulatory Physiology*. 2004;287(6):H2493-H500.
- 830 25. Guiot C, Todros T, Piantà P, Sciarrone A, Kosanke G, Kaufmann P. The
831 diameter distribution of the stem villi arteries does not discriminate between normal and
832 intra uterine growth restricted placentas. *Computational and Mathematical Methods in*
833 *Medicine*. 1999;1(4):263-73.
- 834 26. Zamir M. *The Physics of Coronary Blood Flow*. New York: Springer; 2005.
- 835 27. Hunt D, Savage VM. Asymmetries arising from the space-filling nature of
836 vascular networks. *arXiv preprint arXiv:150803682*. 2015.
- 837 28. Newberry MG, Ennis DB, Savage VM. Testing Foundations of Biological Scaling
838 Theory Using Automated Measurements of Vascular Networks. *PLoS Comput Biol*.
839 2015;11(8):e1004455.
- 840 29. Zamir M. Nonsymmetrical bifurcations in arterial branching. *The Journal of*
841 *general physiology*. 1978;72(6):837-45.
- 842 30. Zamir M. Optimality principles in arterial branching. *Journal of Theoretical*
843 *Biology*. 1976;62(1):227-51.
- 844 31. Zamir M, Zamir M. *The physics of pulsatile flow*: Springer; 2000.
- 845 32. Murray CD. The Physiological Principle of Minimum Work. I. The Vascular
846 System and the Cost of Blood Volume. *Proc Natl Acad Sci*. 1926;12(3):207-14.
- 847 33. Murray CD. The physiological principle of minimum work applied to the angle of
848 branching of arteries. *The Journal of general physiology*. 1926;9(6):835-41.
- 849 34. Adam JA. Blood vessel branching: beyond the standard calculus problem.
850 *Mathematics Magazine*. 2011;84(3):196-207.
- 851 35. Kassab GS, Imoto K, White FC, Rider CA, Fung YC, Bloor CM. Coronary arterial
852 tree remodeling in right ventricular hypertrophy. *Am J Physiol*. 1993;265:H366-H75.
- 853 36. Kassab GS, Rider CA, Tang NJ, Fung YB. Morphometry of Pig Coronary Arterial
854 Trees. *Am J Physiol*. 1993;265.
- 855 37. Zamir M, Chee H. Segment analysis of human coronary arteries. *Journal of*
856 *Vascular Research*. 1987;24(1-2):76–84.
- 857 38. Yen MRT, Zhuang FY, Fung YC, Ho HH, Tremer H, Sabin SS. Morphometry of
858 the cat's pulmonary arteries. *J Biomech Eng* 1984;106:131-6.
- 859 39. Newberry M. Code for angicart software 2011 [Available from:
860 github.com/mnewberry/angicart].
- 861 40. Yao Y, Jumabay M, Wang A, Boström KI. Matrix Gla protein deficiency causes
862 arteriovenous malformations in mice. *The Journal of clinical investigation*.
863 2011;121(8):2993-3004.

- 864 41. Price CA, Symonova O, Mileyko Y, Hilley T, Weitz JS. Leaf extraction and
865 analysis framework graphical user interface: Segmenting and analyzing the structure of
866 leaf veins and areoles. *Plant Physiology*. 2011;155(1):236.
- 867 42. Mileyko Y, Edelsbrunner H, Price CA, Weitz JS. Hierarchical ordering of reticular
868 networks. *PLoS One*. 2012;in press.
- 869 43. Scoffoni C, Rawls M, McKown A, Cochard H, Sack L. Decline of leaf hydraulic
870 conductance with leaf hydration: relationship to leaf size and venation architecture.
871 *Plant Physiology*. 2011;156:832-43.
- 872 44. Krogh A. The Supply of Oxygen to the Tissues and the Regulation of the
873 Capillary Circulation. *Journal of Physiology*. 1919;52(6):457-74.
- 874 45. Krogh A. The Rate of Diffusion of Gases through Animal Tissues, with Some
875 Remarks on the Coefficient of Invasion. *Journal of Physiology*. 1919;52(6):391-408.
- 876 46. Greenberg I, Robertello RA. The three factory problem. *Mathematics Magazine*.
877 1965;38(2):67-72.
- 878 47. Van de Lindt W. A geometrical solution of the three factory problem. *Mathematics
879 Magazine*. 1966;39(3):162-5.
- 880 48. Shen Y, Tolosa J. The weighted fermat triangle problem. *International Journal of
881 Mathematics and Mathematical Sciences*. 2008;2008.
- 882 49. Fung YC. *Biodynamics*. New York: Springer Verlag; 1984.
- 883 50. Fung YC. *Biomechanics: Motion, Flow, Stress, and Growth*. New York: Springer-
884 Verlag; 1990.
- 885 51. Zamir M, Wrigley SM, Langille BL. Arterial Bifurcations in the Cardiovascular
886 System of a Rat. *J Gen Physiol*. 1983;81:325-35.
- 887 52. Guo Y, Chen TH, Zeng X, Warburton D, Boström KI, Ho CM, et al. Branching
888 patterns emerge in a mathematical model of the dynamics of lung development. *The
889 Journal of physiology*. 2014;592(2):313-24.
- 890 53. Metzger RJ, Klein OD, Martin GR, Krasnow MA. The branching programme of
891 mouse lung development. *Nature*. 2008;453:745-51.
- 892 54. Jakulin A, Bratko I, editors. Testing the significance of attribute interactions.
893 Proceedings of the twenty-first international conference on Machine learning; 2004:
894 ACM.
- 895 55. Bettencourt LMA, Hand J, Lobo J. Santa Fe Institute Working Papers. 2015.
- 896

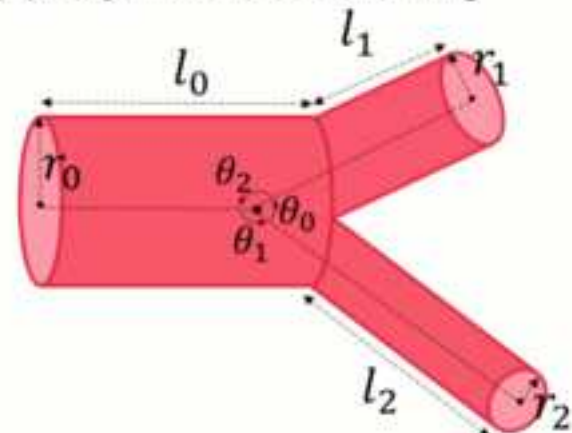
(a) Mouse lung

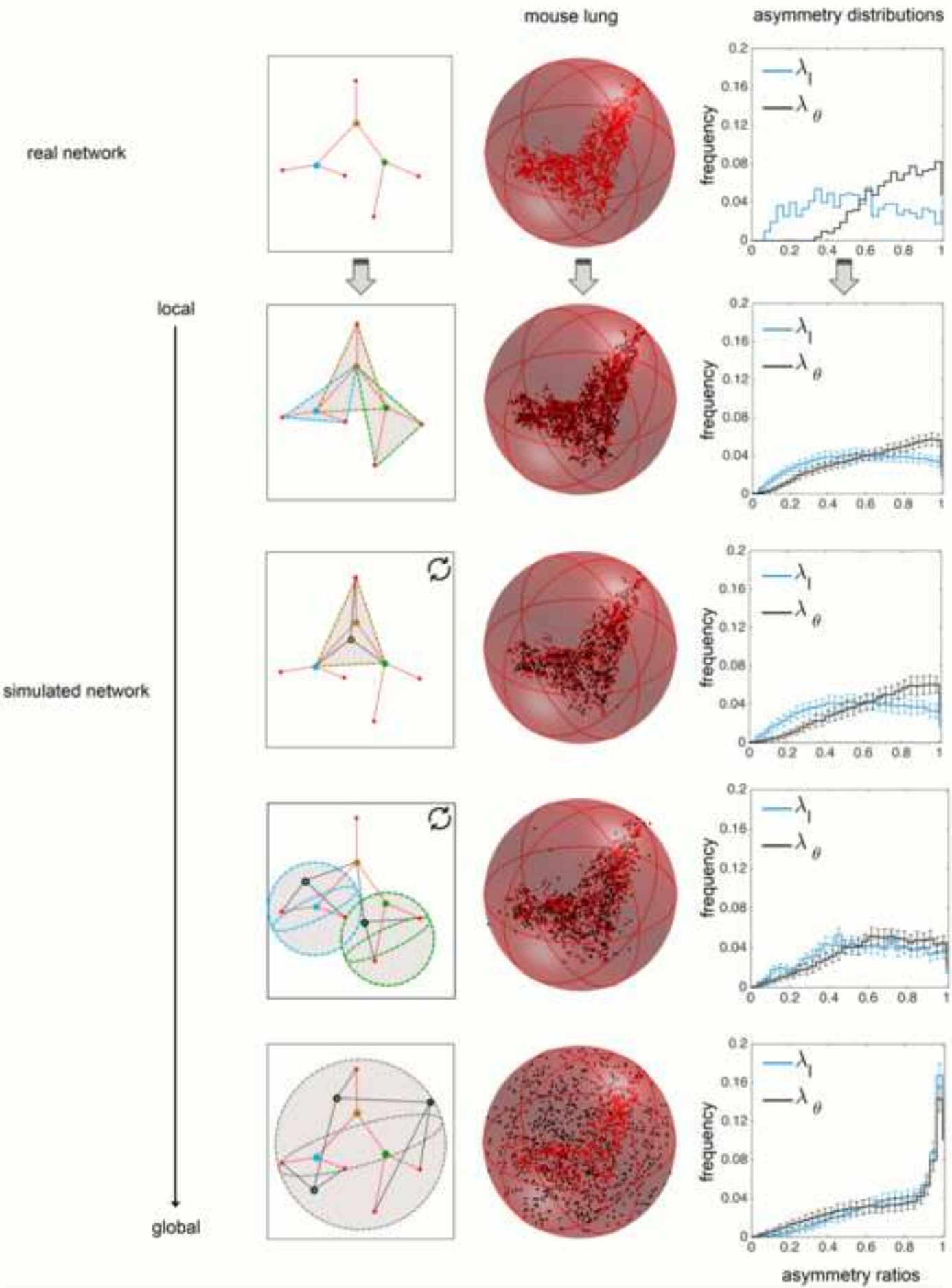


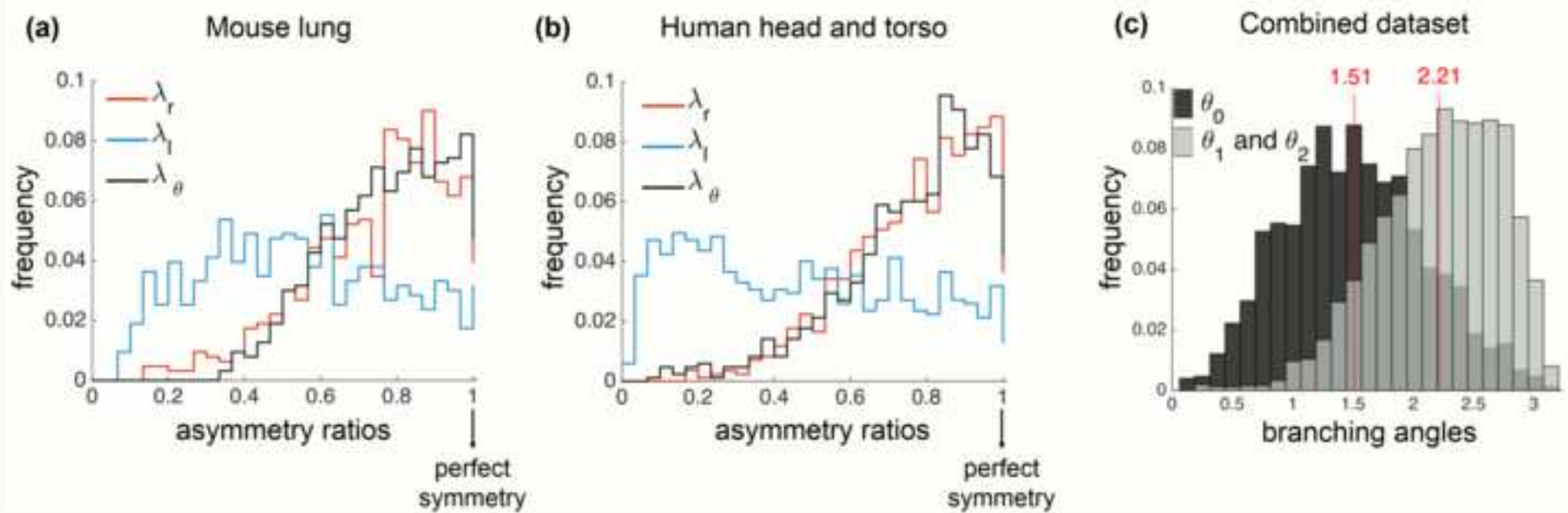
(b) Human head and torso

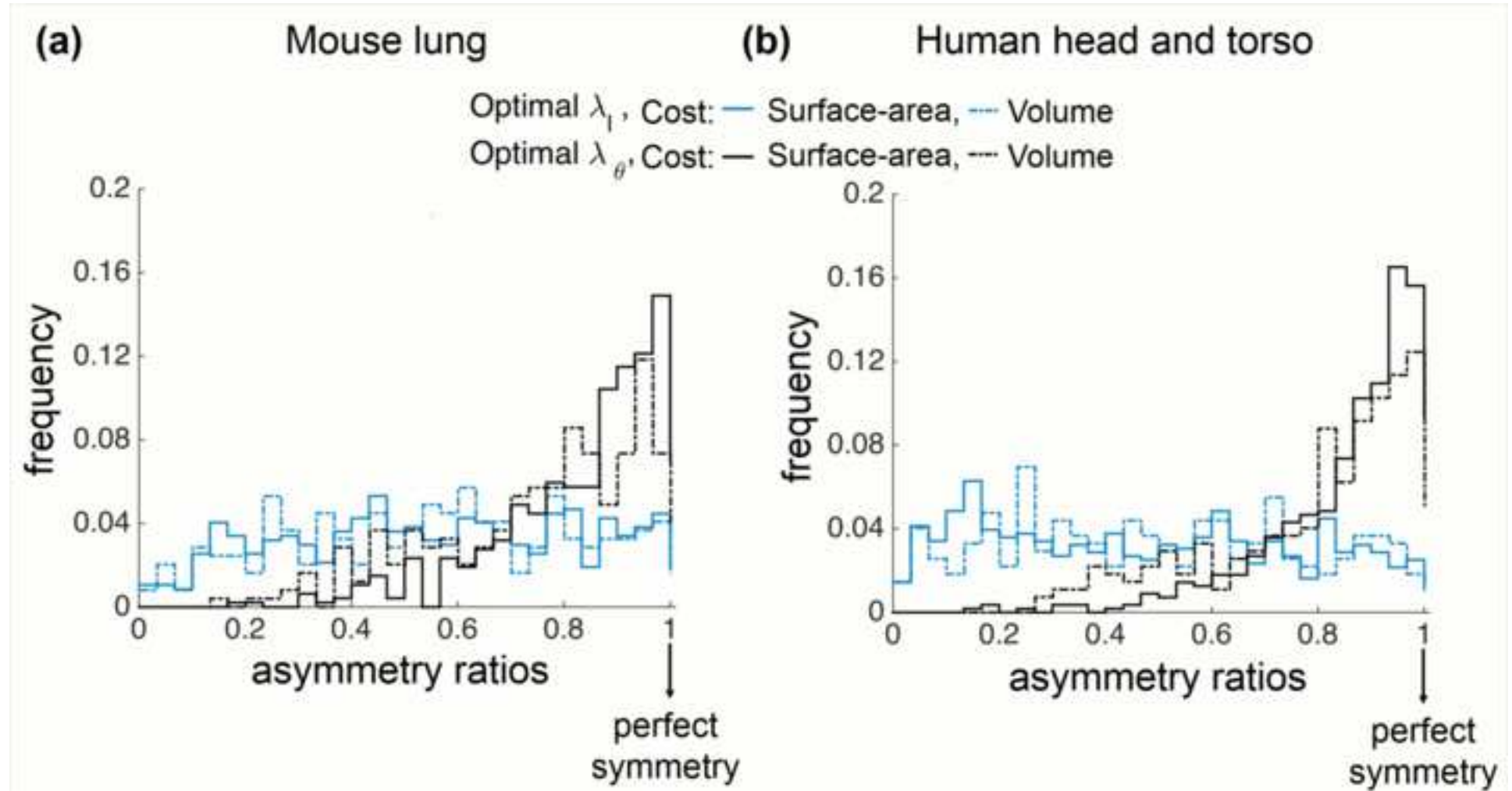


(c) Asymmetric branching





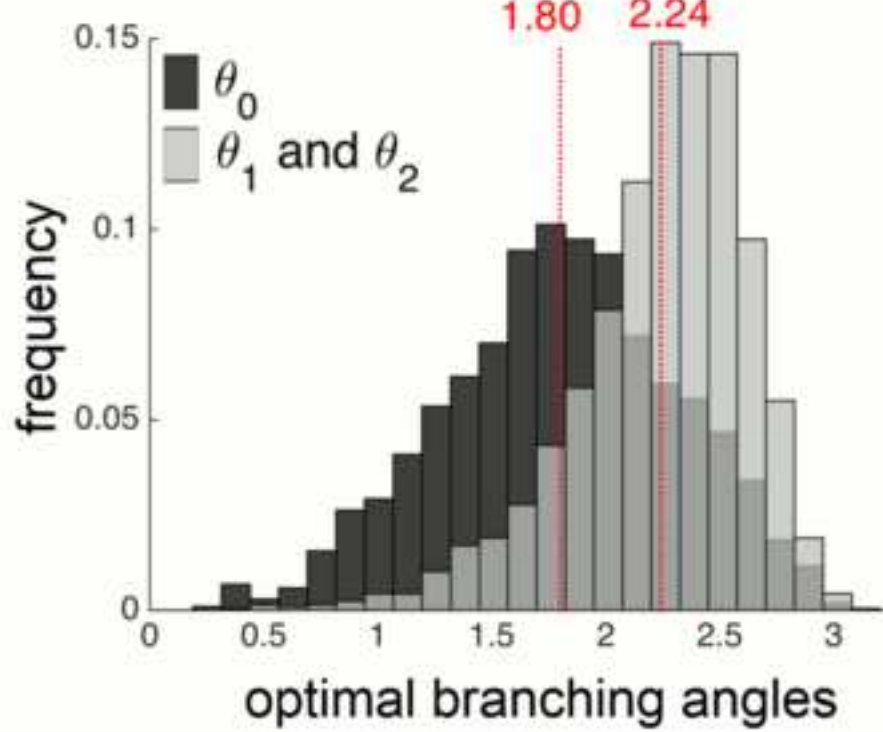




Combined Data

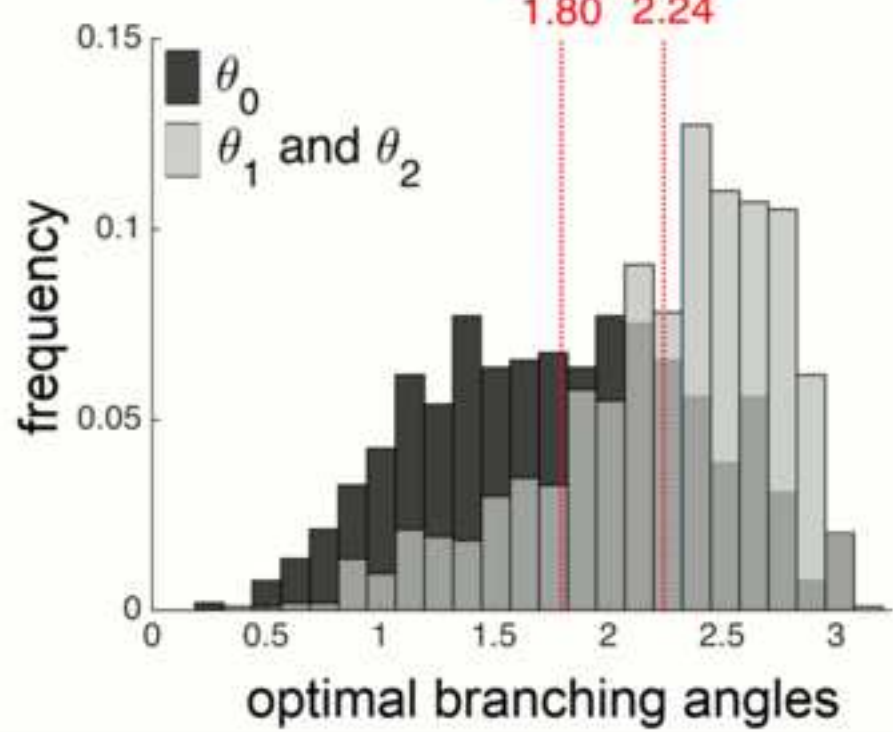
(a)

Cost: Surface-area



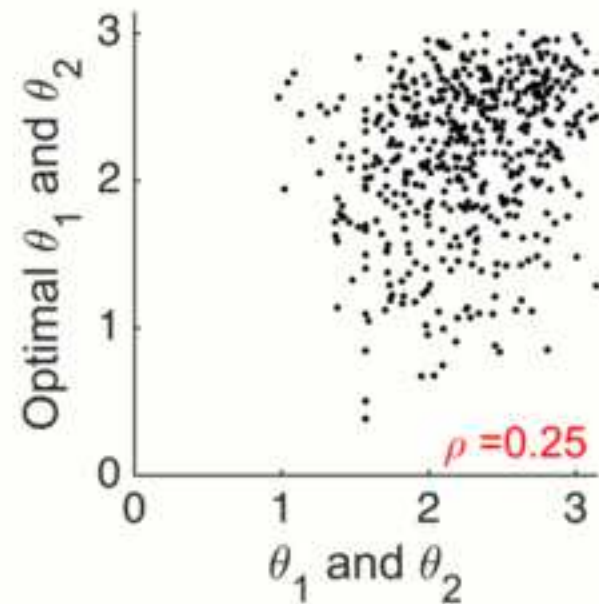
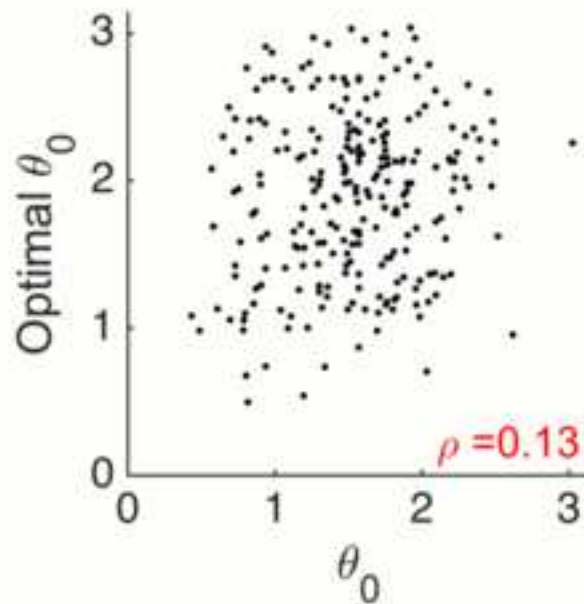
(b)

Cost: Volume



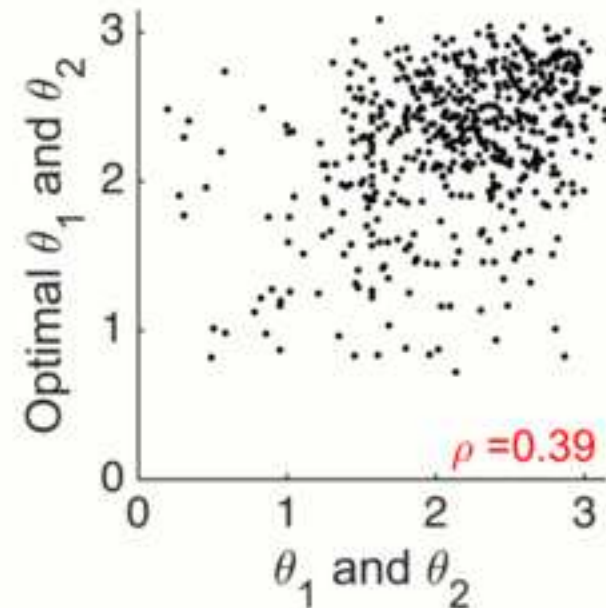
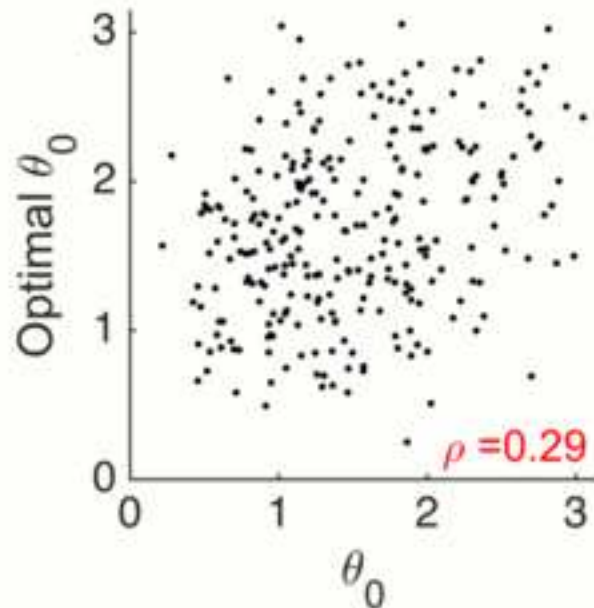
(a)

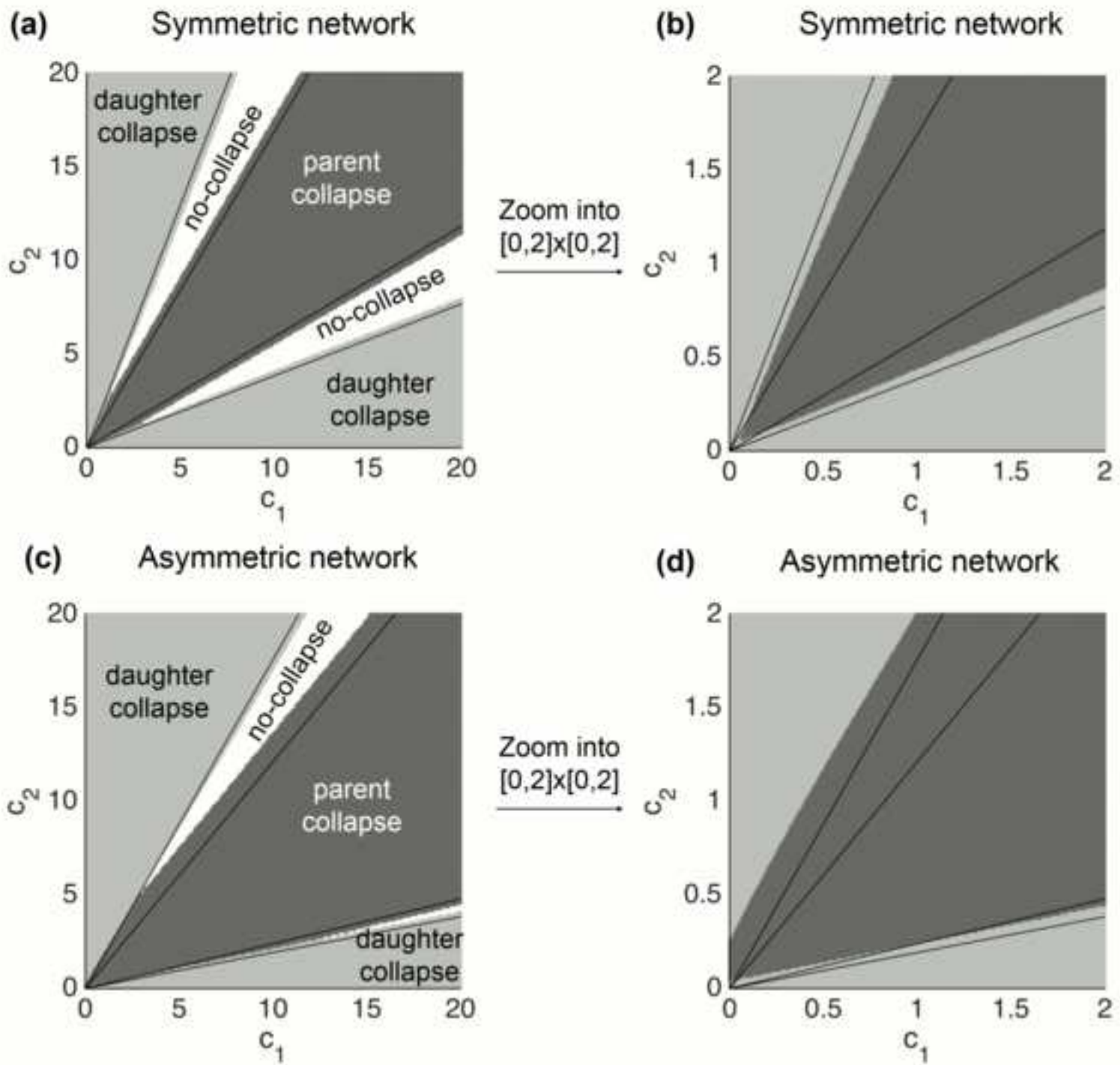
Mouse lung, Cost: Volume



(b)

Human head and torso, Cost: Volume







Click here to access/download
Supporting Information
SI captions .pdf





Click here to access/download
Supporting Information
Fig S1.tiff





Click here to access/download
Supporting Information
Fig S2.tiff





Click here to access/download
Supporting Information
Fig S3.tiff





Click here to access/download
Supporting Information
Fig S4.tiff





Click here to access/download
Supporting Information
Fig S5.tiff





Click here to access/download
Supporting Information
Fig S6.tiff





Click here to access/download
Supporting Information
Fig S7.tiff





Click here to access/download
Supporting Information
Fig S8.tiff





Click here to access/download
Supporting Information
Table S1.pdf



Click here to access/download
Supporting Information
Text S1.pdf





Click here to access/download
Other
Appendix.pdf



Click here to access/download

Related Manuscript
Newberry_PLOS comp bio.PDF



Click here to access/download
Related Manuscript
Hunt_Arxiv.pdf